JCB Journal of Cell Biology

ARTICLE

A PINCH-1–Smurf1 signaling axis mediates mechano-regulation of BMPR2 and stem cell differentiation

Ling Guo[1*], Rong Wang[1*], Kuo Zhang[1*], Jifan Yuan[1], Jiaxin Wang[1], Xiaoxia Wang[1], Jianfei Ma[1], and Chuanyue Wu[2]

Mechano-environment plays multiple critical roles in the control of mesenchymal stem cell (MSC) fate decision, but the underlying signaling mechanisms remain undefined. We report here a signaling axis consisting of PINCH-1, SMAD specific E3 ubiquitin protein ligase 1 (Smurf1), and bone morphogenetic protein type 2 receptor (BMPR2) that links mechano-environment to MSC fate decision. PINCH-1 interacts with Smurf1, which inhibits the latter from interacting with BMPR2 and consequently suppresses BMPR2 degradation, resulting in augmented BMP signaling and MSC osteogenic differentiation (OD). Extracellular matrix (ECM) stiffening increases PINCH-1 level and consequently activates this signaling axis. Depletion of PINCH-1 blocks stiff ECM-induced BMP signaling and OD, whereas overexpression of PINCH-1 overrides signals from soft ECM and promotes OD. Finally, perturbation of either Smurf1 or BMPR2 expression is sufficient to block the effects of PINCH-1 on BMP signaling and MSC fate decision. Our findings delineate a key signaling mechanism through which mechano-environment controls BMPR2 level and MSC fate decision.

Introduction

Proper control of stem cell fate decision is crucial for embryonic development, tissue homeostasis, repair, and regeneration. Stem cell differentiation is regulated by multiple signaling pathways, including those of TGFβ/bone morphogenetic protein (BMP), integrin, Hippo, Wnt, and FGFs (Blank et al., 2008; Chen et al., 2016). Furthermore, there are extensive cross talks between these signaling pathways, which, collectively, determine the final outcome of stem cell fate decision. Importantly, stem cell differentiation is controlled by not only biochemical, but also mechanical signals from extracellular environment or niche (Vogel and Sheetz, 2009; Dupont et al., 2011; MacQueen et al., 2013; Chen et al., 2016; Vining and Mooney, 2017). Pioneering studies by McBeath et al. (2004) have shown that mesenchymal stem cell (MSC) fate decision is regulated by cell shape and cytoskeletal tension. Furthermore, changes in ECM stiffness have been found to exert profound effects on stem cell differentiation (Mammoto and Ingber, 2009; Wozniak and Chen, 2009; Dingal and Discher, 2014). Because of their importance, the signaling mechanisms through which mechano-environment regulates stem cell differentiation are an important area of current biological and medical research.

It has been well documented that BMP signaling pathways are critical for control of stem cell differentiation (Zhang and Li, 2005; Beederman et al., 2013; Wang et al., 2014; Garg et al., 2017). Several BMPs, including BMP2, BMP6, BMP7, and BMP9, have been shown to promote MSC osteoblastic differentiation (Cheng et al., 2003; Noël et al., 2004; Beederman et al., 2013). BMPs exert their effects on cells through interacting with cell surface hetero-tetrameric complexes consisting of two dimers of type I and II serine/threonine kinase receptors, in which the constitutively active type II receptor transphosphorylates the type I receptor, leading to activation of the type I receptor, phosphorylation of Smad1/5/8, and downstream signaling (Shi and Massagué, 2003; Sieber et al., 2009; Miyazono et al., 2010; Gomez-Puerto et al., 2019). BMPR2 is a BMP-specific type 2 receptor that is crucial for embryonic development, vasculogenesis, and osteogenesis (Onishi et al., 1998; Garimella et al., 2007; Lehnerdt et al., 2007; Kim et al., 2017; Andruska and Spiekerkoetter, 2018; Gomez-Puerto et al., 2019). Lack of BMPR2 in mice is lethal in the early embryonic stage (Beppu et al., 2000), while mice expressing a BMPR2 mutant with reduced signaling capability die at midgestation with cardiovascular and skeletal defects (Délot et al.,

[1]Guangdong Provincial Key Laboratory of Cell Microenvironment and Disease Research, Shenzhen Key Laboratory of Cell Microenvironment, Academy for Advanced Interdisciplinary Studies and Department of Biology, Southern University of Science and Technology, Shenzhen, China; [2]Department of Pathology, University of Pittsburgh School of Medicine, Pittsburgh, PA.

*L. Guo, R. Wang, and K. Zhang contributed equally to this paper; Correspondence to Chuanyue Wu: carywu@pitt.edu; Ling Guo: guol@sustc.edu.cn.

https://doi.org/10.1083/jcb.201902022

2003). BMPR2 is critically involved in promoting MSC differentiation toward osteoblastic lineage (Wu et al., 2010; Yang et al., 2010; Zeng et al., 2012; Cao et al., 2015; Kim et al., 2017). Interestingly, overexpression of Smurf1, a C2-WW-HECT domain E3 ubiquitin ligase (Zhu et al., 1999), in HEK239T cells reduced the level of BMPR2 (Murakami et al., 2010). It remains to be determined, however, whether Smurf1 mediates BMPR2 degradation in MSCs and, if so, whether it mediates the upstream signals and the molecular mechanism that controls this process.

Another signaling pathway that is critical for control of stem cell differentiation is that of integrins, transmembrane receptors mediating cell-ECM adhesion and signaling (Schwartz, 2010; Yim and Sheetz, 2012; Humphrey et al., 2014; Horton et al., 2016). PINCH-1 is a widely expressed and evolutionally conserved cytoplasmic component of the integrin signaling pathway (Tu et al., 1999; Zhang et al., 2002; Wu, 2004, 2005; Legate et al., 2006; Kovalevich et al., 2011). In this study, we show that Smurf1 binds BMPR2 and controls its degradation in MSCs in response to mechanical signals from ECM. Furthermore, we identify PINCH-1 as a key regulator of Smurf1-mediated binding and degradation of BMPR2 in MSC differentiation, suggesting a cross talk between the integrin and BMP signaling pathways in this process. Mechanistically, PINCH-1 binds directly to the Smurf1 C2 domain, to which BMPR2 binds. Overexpression of PINCH-1 inhibited the Smurf1–BMPR2 interaction and consequently Smurf1-mediated degradation of BMPR2. Conversely, depletion of PINCH-1 increased Smurf1-mediated binding and degradation of BMPR2. Notably, ECM stiffening increased PINCH-1 level and its complex formation with Smurf1, resulting in inhibition of Smurf1 interaction and degradation of BMPR2 and consequently augmented BMP signaling and osteogenic differentiation (OD). Depletion of PINCH-1 was sufficient to inhibit the ECM stiffening–induced increase of BMPR2 signaling and OD, whereas overexpression of PINCH-1 blocked ECM softening–induced degradation of BMPR2 and adipogenic differentiation (AD). These results identify a novel PINCH-1–Smurf1 signaling axis that links mechano-environment to BMPR2 degradation and MSC fate decision.

Results

PINCH-1 is critical for control of MSC differentiation

In our investigation of MSC differentiation, we noticed that PINCH-1 protein level was increased during OD (Fig. 1 A). PINCH-1 mRNA level, however, was not increased under the same condition (Fig. 1 B). PINCH-1 level was more than doubled soon after (within 1 d) induction of OD and was tripled by day 4 (Fig. 1 A). The levels of BMPR2 and phosphor-Smad1/5 were also increased, albeit the increases initially lagged behind those of PINCH-1 level (Fig. 1 A). No increases of BMPR2 mRNA (Fig. 1 B) or BMPR1A and Smad1 levels (Fig. 1 A) were observed under the same condition.

To test whether the increase of PINCH-1 level is functionally important, we depleted PINCH-1 from MSCs (Fig. 1 C, lane 3). PINCH-1–deficient MSCs, unlike control MSCs expressing a normal level of PINCH-1, were unable to undergo OD when cultured under OD condition (Fig. 1, D–F). Furthermore, depletion of PINCH-1 was sufficient to induce spontaneous AD in MSCs cultured under normal growth condition (Fig. 1, I and J) and enhance AD in MSCs cultured under AD condition (Fig. 1, D, G, and H). Reexpression of 3xFLAG-tagged PINCH-1 (3f-P1) in PINCH-1–deficient MSCs (Fig. 1 C, lane 5) effectively reversed the differentiation defects induced by depletion of PINCH-1 (Fig. 1, D–H). To test the function of PINCH-1 in MSC differentiation in vivo, we transplanted PINCH-1–deficient MSCs and control MSCs into mice and analyzed their abilities to differentiate into osteoblasts or adipocytes. The tissues were dissected from the mouse recipients and analyzed by hematoxylin and eosin (H&E) staining (Fig. 2 A). Western blotting (WB) analyses confirmed that PINCH-1 level in the tissues derived from PINCH-1 knockdown MSCs was significantly lower than that in control MSCs (Fig. 2 B). Consistent with the results in cell culture, depletion of PINCH-1 markedly inhibited OD (Fig. 2 C) and concomitantly increased AD (Fig. 2 D) in vivo. Collectively, these results suggest that PINCH-1 level is critical for control of MSC fate decision (i.e., higher levels of PINCH-1 favor OD, whereas lower levels of PINCH-1 favor AD).

PINCH-1 regulates BMPR2 level and its downstream signaling

We next sought to determine the mechanism by which PINCH-1 regulates MSC differentiation. Because the increase of BMPR2 followed that of PINCH-1 during OD (Fig. 1 A), we tested whether the increase of BMPR2 is caused by that of PINCH-1. To do this, we depleted PINCH-1 from the MSCs and found that it significantly reduced BMPR2 protein (Fig. 3 A, compare lane 3 with lanes 1 and 2), but not mRNA level (Fig. 3 B). Knockdown of integrin-linked kinase (ILK) or kindlin-2 did not significantly reduce BMPR2 level (Fig. S1). Consistent with our previous studies (Guo et al., 2018), knockdown of kindlin-2 did reduce the level of YAP1 (Fig. S1). In contrast to a marked reduction of BMPR2 level, depletion of PINCH-1 did not significantly change the levels of BMPR1A and Smad1 (Fig. 3 A) or Rac1 activity (Fig. 3 C). Consistent with the reduction of BMPR2 level, the level of Smad1/5 phosphorylation was also reduced in response to depletion of PINCH-1 (Fig. 3 A). To further test this, we reexpressed 3f-P1 in PINCH-1 knockdown MSCs and found that it substantially increased BMPR2 and phosphor-Smad1/5 levels (Fig. 3 D). Additionally, knockdown of PINCH-1 diminished nuclear localization of phosphor-Smad1/5, which was restored by reexpression of 3f-P1 (Fig. 3 F). Similar results were obtained with a BMP reporter containing BMP-responsive elements (BREs) fused to a luciferase reporter gene (Korchynskyi and ten Dijke, 2002; Yadav et al., 2012; Fig. 3 E). These results demonstrate that PINCH-1 is critical for regulation of BMPR2 level and its downstream signaling.

Down-regulation of BMPR2 expression is responsible for PINCH-1 deficiency–induced inhibition of OD

We next tested whether the down-regulation of BMPR2 expression is responsible for PINCH-1 deficiency–induced inhibition of OD. To do this, we overexpressed 3xFLAG-tagged BMPR2 (3f-BMPR2) in PINCH-1–deficient MSCs (Fig. 4 A, lane 4) as well as normal MSCs (Fig. S2 A, lane 3) and assessed the effects on Smad1/5 phosphorylation and MSC differentiation. Consistent

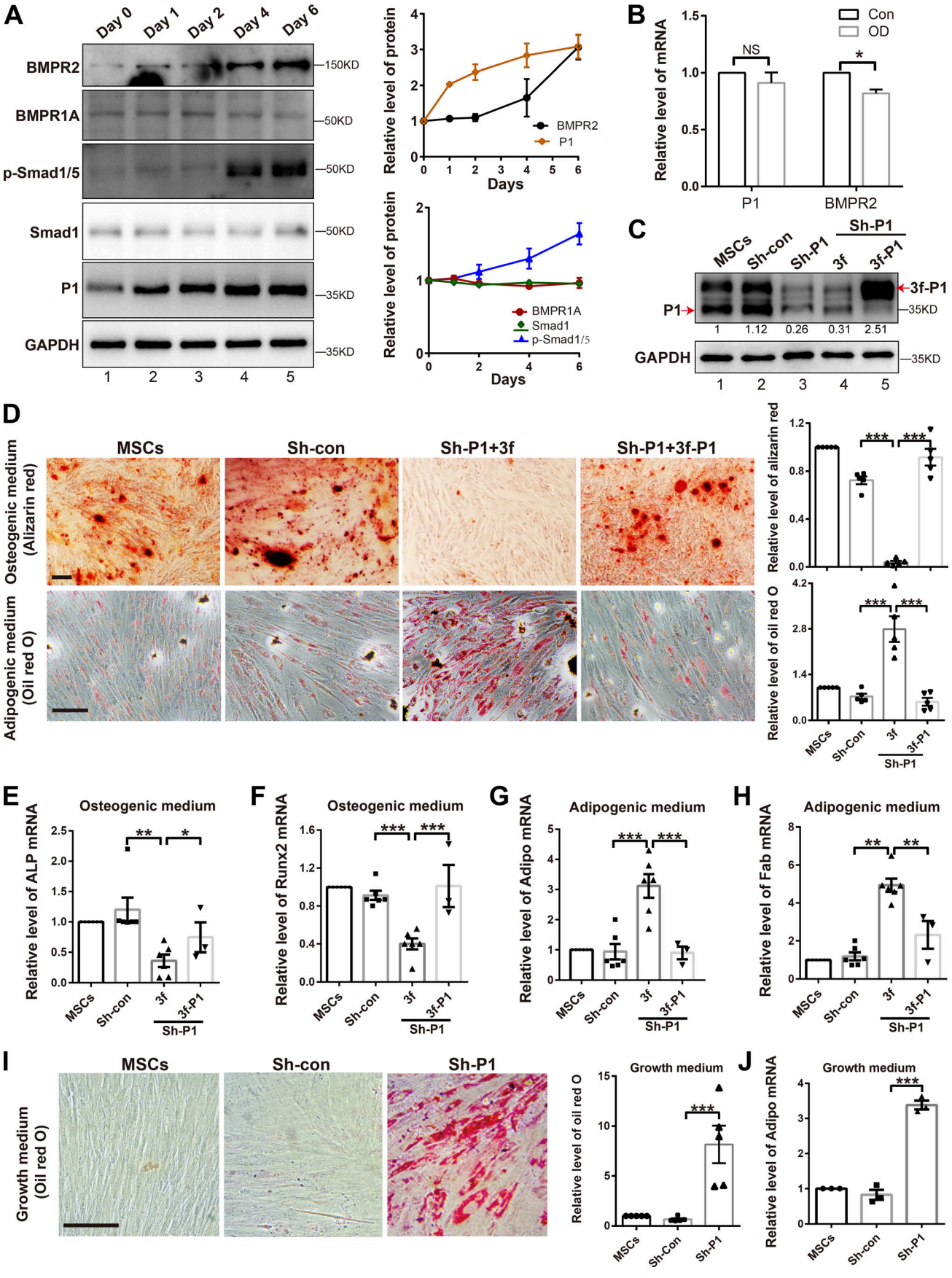

Figure 1. **PINCH-1 is critical for control of MSC differentiation. (A)** hMSCs were cultured under OD medium and analyzed by WB. Right: The protein levels at 1, 2, 4, and 6 d were quantified and compared with those at day 0 (normalized to 1, $n = 3$). **(B)** The mRNA levels of PINCH-1 (P1) and BMPR2 in hMSCs cultured in OD medium for 6 d were analyzed by RT-PCR and compared with those in normal medium (normalized to 1, $n = 3$). **(C–H)** hMSCs were infected with control (Sh-con) or PINCH-1 shRNA (Sh-P1) lentivirus. **(C)** 2 d later, the Sh-P1 infectants were infected with lentivirus encoding 3f-P1 or 3xFLAG only (3f) for 3 d and analyzed by WB. The intensities of P1 or 3f-P1 bands from the infectants were quantified, compared with that of P1 in uninfected hMSCs (normalized to 1), and indicated under the protein bands. **(D)** The cells were cultured in OD or AD medium for 14 d and then stained with Alizarin red S or oil red O. Right: Alizarin red S– or oil red O–positive areas in the infectants were quantified and compared with those in uninfected hMSCs (normalized to 1). Scale bars = 100 µm. **(E–H)** The mRNA levels of OD markers ALP and Runx2 (E and F) and AD markers Adipo and Fab (G and H) in the infected hMSCs were analyzed by RT-PCR and compared with those of uninfected MSCs (normalized to 1, $n \geq 3$). **(I and J)** Spontaneous AD of PINCH-1 knockdown hMSCs. hMSCs were infected with Sh-P1 or Sh-con lentivirus, cultured in normal medium for 14 d, and stained with oil red O. Scale bar = 100 µm. **(I)** Right: Oil red O–positive areas in the infectants were quantified and compared with those in uninfected hMSCs (normalized to 1). **(J)** The mRNA levels of Adipo in the PINCH-1 knockdown and Sh-con control cells were analyzed by RT-PCR and compared with those in uninfected hMSCs (normalized to 1, $n = 3$). Data represent mean ± SEM. Statistical significance was calculated using one-way ANOVA with Tukey–Kramer post-hoc analysis (D–J) or two-tailed unpaired Student's *t* test (B), *P < 0.05; **P < 0.01; ***P < 0.001.

with previous studies (Wu et al., 2010; Yang et al., 2010; Zeng et al., 2012; Cao et al., 2015; Kim et al., 2017), overexpression of 3f-BMPR2 enhanced Smad1/5 phosphorylation (Fig. S2 A), resulting in augmented OD and reduced AD (Fig. S2, B–F). Overexpression of 3f-BMPR2 in PINCH-1–deficient MSCs effectively restored the defects on Smad1/5 phosphorylation (Fig. 4 A), nuclear localization (Fig. 4 C), BMP reporter activity (Fig. 4 B), and OD (Fig. 4, D–F) and suppressed PINCH-1 deficiency–induced AD (Fig. 4, D, G, and H). Collectively, these results suggest that PINCH-1 regulates MSC differentiation through, at least in part, control of BMPR2 level.

PINCH-1 controls BMPR2 level through regulation of Smurf-1–mediated degradation of BMPR2

We next sought to determine the mechanism by which PINCH-1 regulates BMPR2 level. Because PINCH-1 regulates BMPR2 protein but not mRNA level (Fig. 3, A and B) and previous studies in HEK293 cells have implicated a role of Smurf1 in BMPR2 degradation (Murakami et al., 2010), which we have confirmed (Fig. S3), we tested the possibility that Smurf1 is involved in PINCH-1 regulation of BMPR2 level in MSCs. To do this, we overexpressed Smurf1, and used a different E3 ubiquitin ligase NEDD4 as a control, in MSCs. Overexpression of Smurf1 (Fig. 5 A, compare lane 3 with lanes 1 and 2), but not that of NEDD4 (Fig. 5 B, compare lane 3 with lanes 1 and 2), markedly reduced the level of BMPR2, which was reversed by the presence of proteasome inhibitor MG132 or lysosomal inhibitor leupeptin (Fig. S4 A). Conversely, depletion of Smurf1 from MSCs increased BMPR2 level (Fig. 5 C, compare lane 3 with lanes 1 and 2). Neither overexpression nor knockdown of Smurf1 significantly altered PINCH-1 level (Fig. 5, A and C).

Next, we sought to test whether Smurf1 binds BMPR2 and, if so, the Smurf1 domain responsible for the binding. Because overexpression of WT Smurf1 diminished BMPR2 level (Fig. 5 A, lane 3), we expressed a 3xFLAG-tagged catalytically inactive Smurf1 mutant CA (3f-CA; Wei et al., 2017), in which Cys^{699} within the catalytic HECT domain is substituted with Ala, in MSCs and tested its complex formation with BMPR2 by coimmunoprecipitation (coIP). The results showed that BMPR2 was indeed coimmunoprecipitated with 3f-CA (Fig. 5 D, lane 4). In control experiments, Smurf1-binding protein kindlin-2 (Wei et al., 2017), but not irrelevant protein GAPDH, was also coimmunoprecipitated with 3f-CA (Fig. 5 D, lane 4), confirming the specificity of the experiments. To further test this, we analyzed the interaction between 3f-CA and BMPR2 using proximity ligation assay (PLA). Kindlin-2 and irrelevant protein Ki-67 were used as positive and negative controls, respectively. The results showed that BMPR2 and 3f-CA (Fig. 5 E), like kindlin-2 and Smurf1 (Fig. S5 A) but not Ki-67 and Smurf1 (Fig. S5 B), formed a complex in MSCs. To test whether Smurf1 binds BMPR2 directly, we expressed recombinant MBP-BMPR2 cytoplasmic domain (CD; residues 203–1,038) and GST-Smurf1, respectively. GST-tagged dynein light chain tctex-1 (DYNLT), which is known to bind BMPR2 CD (Machado et al., 2003), and GST-tagged NEDD4, the overexpression of which does not reduce BMPR2 level (Fig. 5 B), were used as positive and negative controls, respectively. Consistent with the coIP and PLA experiments, GST-Smurf1 (Fig. 5 F, lane 4), but not GST (Fig. 5 F, lane 2), readily pulled down MBP-BMPR2-CD, suggesting that Smurf1 directly interacts with BMPR2 CD. In control experiments, MBP-BMPR2-CD was pulled down by GST-DYNLT (Fig. 5 F, lane 8) but not GST-NEDD4 (Fig. 5 F, lane 6), confirming the specificity of the assay. To further test this, we generated MBP-BMPR2 kinase domain (KD; residues 203–504) and tested its Smurf1 binding. The results showed that GST-Smurf1 (Fig. 5 G, lane 4), but neither GST (Fig. 5 G, lane 2) nor GST-NEDD4 (Fig. 5 G, lane 6), readily pulled down MBP-BMPR2-KD, suggesting that BMPR2 KD located within the CD is sufficient to bind Smurf1. To map the Smurf1 domain that mediates BMPR2 binding, we generated GST fusion proteins containing the various domains (C2, WW, or HECT) of Smurf1. GST-C2 (Fig. 5 H, lane 4), but neither GST-WW (Fig. 5 H, lane 6) nor GST-HECT (Fig. 5 H, lane 8), pulled down MBP-BMPR2-CD. Similarly, GST-C2 (Fig. 5 I, lane 4), but neither GST-WW (Fig. 5 I, lane 6) nor GST-HECT (Fig. 5 I, lane 8), pulled down MBP-BMPR2-KD. Next, we expressed FLAG-tagged Smurf1 mutant in which the C2 domain is deleted (3f-ΔC2) in MSCs (Fig. 5 D, lane 6) and confirmed that 3f-ΔC2 (Fig. 5 D, lane 8), unlike 3f-CA (Fig. 5 D, lane 4), failed to coimmunoprecipitate BMPR2. Collectively, these results suggest that the Smurf1 C2 domain and BMPR2 KD are involved in mediating the Smurf1–BMPR2 interaction.

To test whether BMPR2 binding is required for Smurf1-mediated degradation of BMPR2, we expressed FLAG-tagged WT Smurf1, catalytically inactive CA mutant, BMPR2 binding–defective ΔC2 mutant, and ΔWW mutant in HEK293 cells. As expected, overexpression of WT Smurf1 reduced BMPR2 level

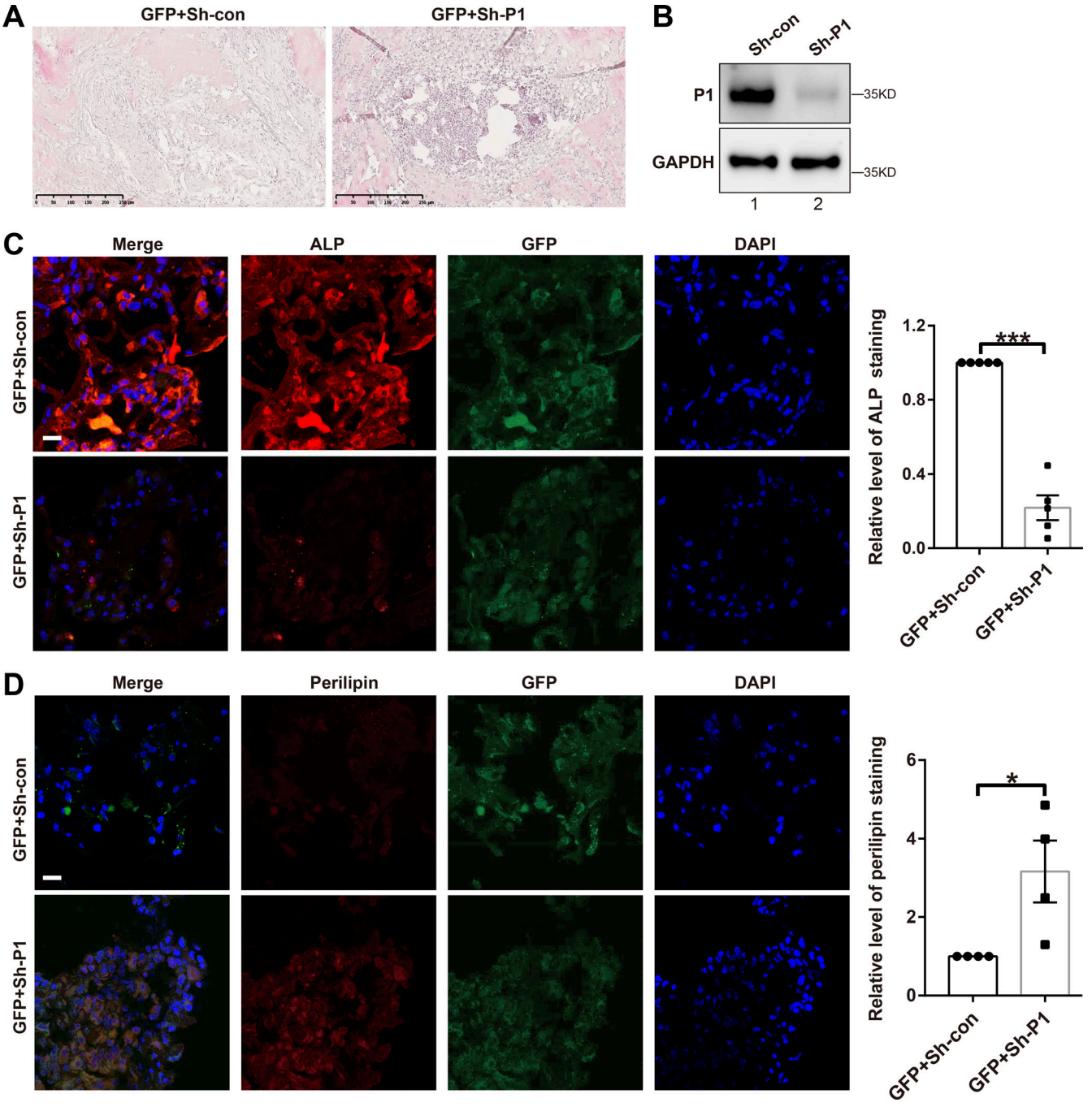

Figure 2. **PINCH-1 regulates MSC differentiation in vivo.** GFP-labeled hMSCs infected with Sh-P1 or Sh-con lentivirus were implanted subcutaneously into Nu/Nu mice. **(A–D)** The tissues were dissected from the mouse recipients 10 d later and analyzed by H&E staining (A; scale bars = 250 µm), WB (B), and IF staining with DAPI and anti-ALP (C) or anti-perilipin (D) Abs. Scale bars = 50 µm. **(C and D)** Right: The mean fluorescence intensities of ALP and perilipin staining in Sh-P1 infectants were quantified and compared with those of Sh-con infectants (normalized to 1). Data represent mean ± SEM. Statistical significance was calculated using two-tailed unpaired Student's *t* test, *P < 0.05; ***P < 0.001.

(Fig. 5 J, compare lanes 1 and 2). Importantly, overexpression of BMPR2 binding-defective ΔC2 (Fig. 5 J, lane 3), like that of catalytically inactive CA (Fig. 5 J, lane 5), failed to reduce BMPR2 level. By marked contrast, overexpression of ΔWW, which contains C2 and HECT domains but lacks WW domain, effectively reduced BMPR2 level (Fig. 5 J, lane 4). These results suggest that the BMPR2-binding C2 domain and the catalytic HECT domain are necessary for Smurf1-mediated degradation of BMPR2.

We next tested whether Smurf1 is involved in PINCH-1 deficiency–induced reduction of BMPR2 level. To do this, we depleted Smurf1 and found that it reversed PINCH-1 deficiency–induced reduction of BMPR2 level (Fig. 6 A). Consistent with this, treatment of cells with MG132 or leupeptin reversed

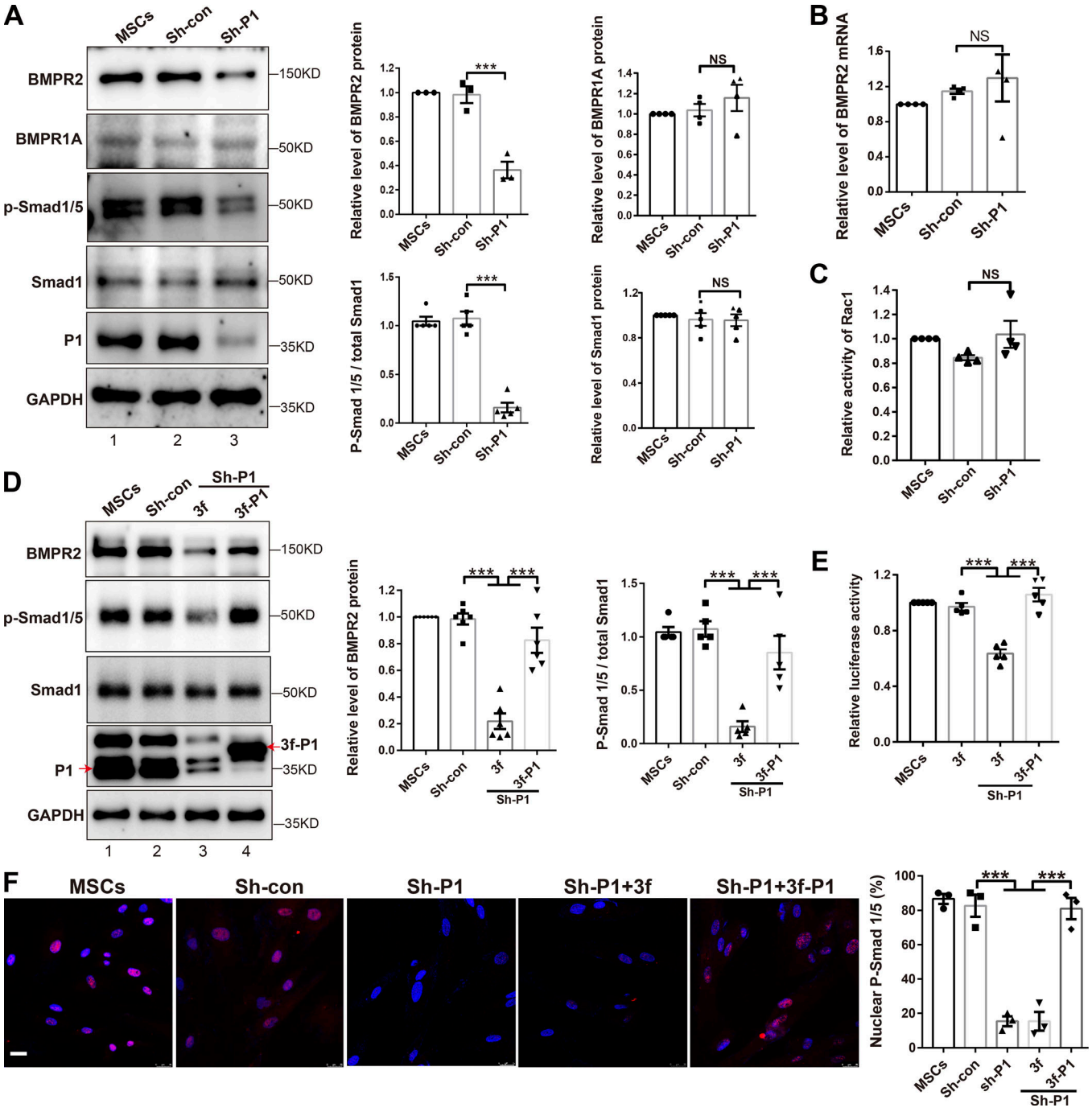

Figure 3. **PINCH-1 regulates BMPR2 level and its downstream signaling. (A)** hMSCs were infected with Sh-P1 or Sh-con lentivirus, cultured in normal medium for 5 d, and analyzed by WB. Right: The protein levels in the infected hMSCs were quantified and compared with those in uninfected hMSCs (normalized to 1, $n \geq 3$). **(B)** The mRNA levels of BMPR2 in the Sh-P1 or Sh-con cells were analyzed by RT-PCR and compared with those of uninfected hMSCs (normalized to 1, $n = 3$). **(C)** Rac1 activities in Sh-P1 or Sh-con cells were analyzed using G-LISA and compared with those of uninfected hMSCs (normalized to 1, $n = 4$). **(D)** hMSCs were infected with Sh-con or Sh-P1 for 2 d, and the Sh-P1 infectants were then infected with 3f or 3f-P1 lentivirus. 3 d later, the cells were analyzed by WB. Right: The protein levels in the infected hMSCs were quantified and compared with those in the uninfected hMSCs (normalized to 1, $n \geq 3$). Red arrows indicate the positions of P1 and 3f-P1. **(E)** hMSCs were infected with BRE-Luc lentivirus for 2 d and then infected with 3f or 3f-P1 lentivirus. 2 d later, the cells were infected with Sh-P1 for 5 d, and BMP reporter activity was assessed by measuring luciferase activity in the infected cells and compared with that in the reporter cells not infected with 3f or 3f-P1 (normalized to 1, $n = 5$). **(F)** The cells were immunofluorescently stained with DAPI and Abs for p-Smad1/5. Scale bar, 25 µm. Right: The percentages of nuclear p-Smad1/5–positive cells among total cells were quantified ($n = 3$). Data represent mean ± SEM. Statistical significance was calculated using one-way ANOVA with Tukey–Kramer post-hoc analysis, ***P < 0.001.

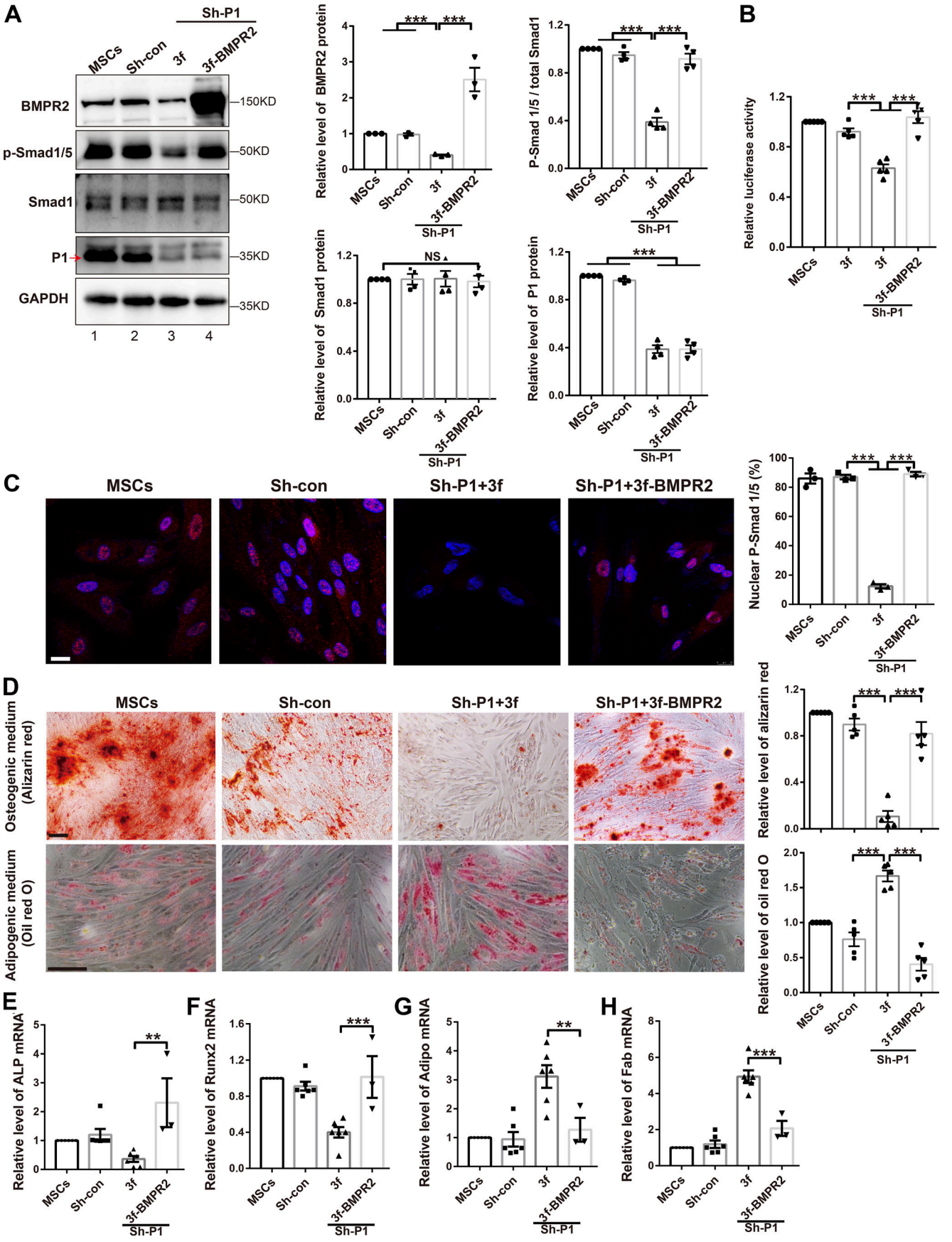

Figure 4. **PINCH-1 regulates MSC differentiation through BMPR2. (A)** hMSCs were infected with Sh-P1 or Sh-con lentivirus for 2 d, and the Sh-P1 infectants were then infected with 3f or 3f-BMPR2 lentivirus. 3 d later, the cells were analyzed by WB. Right: The protein levels in the infected hMSCs were quantified and compared with those in uninfected hMSCs (normalized to 1, $n \geq 3$). **(B)** hMSCs were infected with BRE-Luc lentivirus for 2 d, and the reporter cells were then infected with 3f or 3f-BMPR2 lentivirus. 2 d later, the cells were infected with Sh-P1 lentivirus for 5 d, and BMP reporter activity was assessed by measuring luciferase activity in the cells (as indicated) and compared with that in cells not infected with 3f, 3f-BMPR2, or Sh-P1 (normalized to 1, $n = 5$). **(C)** The cells treated as above (A) were immunofluorescently stained with DAPI and Abs for p-Smad1/5. Scale bar, 25 µm. Right: The percentages of nuclear p-Smad1/5–positive cells among total cells were quantified ($n = 3$). **(D)** The cells were cultured in OD or AD medium for 14 d and stained with Alizarin red S (upper) or oil red O (lower) as indicated. Scale bars = 100 µm. Right: Alizarin red S– or oil red O–positive areas in the infectants were quantified and compared with those in uninfected MSCs (normalized to 1). **(E–H)** The mRNA levels of ALP and Runx2 (E and F) and Adipo and Fab (G and H) in the infected MSCs were analyzed by RT-PCR and compared with those of uninfected MSCs (normalized to 1, $n \geq 3$). Data represent mean ± SEM. Statistical significance was calculated using one-way ANOVA with Tukey–Kramer post-hoc analysis, **P < 0.01; ***P < 0.001.

PINCH-1 deficiency–induced reduction of BMPR2 level (Fig. S4 B), suggesting that proteasome- and lysosome-mediated degradation are involved in PINCH-1 deficiency–induced, Smurf1-mediated reduction of BMPR2 level. As expected, depletion of Smurf1 from PINCH-1–deficient MSCs restored Smad1/5 phosphorylation (Fig. 6 A), nuclear localization (Fig. 6 C), BMP reporter activity (Fig. 6 B), and OD (Fig. 6, D–F). Concomitantly, it suppressed PINCH-1 deficiency–induced AD (Fig. 6, D, G, and H). Collectively, these results suggest that Smurf1 is a key mediator of PINCH-1 in its regulation of BMPR2 expression, signaling, and MSC differentiation.

PINCH-1 interacts with Smurf1 C2 domain and inhibits Smurf1-mediated binding and degradation of BMPR2

We next sought to determine how PINCH-1 regulates Smurf1-mediated degradation of BMPR2. To this end, we first tested whether PINCH-1 interacts with Smurf1. PINCH-1 was readily coimmunoprecipitated with 3f-CA (Fig. 7 A, lane 4). Consistent with this, endogenous Smurf1 and PINCH-1 formed a complex in cells (Fig. 7 B). To test whether they directly interact, we expressed MBP–PINCH-1 and GST-Smurf1, respectively, and tested their binding in a pull-down assay. GST-ILK, which is known to directly bind PINCH-1 (Tu et al., 1999), and α-parvin, an ILK-binding protein that does not directly bind PINCH-1 (Tu et al., 2001; Qin and Wu, 2012), were used as positive and negative controls (Fig. 7 C), respectively. The results showed that MBP–PINCH-1 was pulled down by GST-Smurf1 (Fig. 7 C, lane 4) and GST-ILK (Fig. 7 C, lane 8), but neither GST (Fig. 7 C, lane 2) nor GST-α-parvin (Fig. 7 C, lane 6). To identify the Smurf1 domain mediating PINCH-1 binding, we analyzed the PINCH-1 binding activity of individual Smurf1 domains. GST-C2 (Fig. 7 D, lane 4) and, to a much lesser extent, GST-WW (Fig. 7 D, lane 6), but not GST-HECT (Fig. 7 D, lane 8), bound MBP–PINCH-1. Consistent with this, 3f-ΔC2 (Fig. 7 A, lane 8), unlike 3f-CA (Fig. 7 A, lane 4), failed to coimmunoprecipitate PINCH-1. The findings that PINCH-1 binds to C2, to which BMPR2 also binds (Fig. 5, D, H, and I), raised the possibility that PINCH-1 may inhibit Smurf1 interaction and consequently degradation of BMPR2. To test this, we analyzed the Smurf1–BMPR2 interaction either in the presence or absence of PINCH-1 and found that the presence of MBP–PINCH-1 (Fig. 7 E, lane 8) but not MBP (Fig. 7 E, lane 7) indeed reduced the amount of BMPR2 bound to Smurf1. Furthermore, the binding of BMPR2 to GST-C2 was inhibited by PINCH-1 but not MBP in a dose-responsive manner (Fig. 7 F). Similarly, overexpression of PINCH-1 in cells also reduced the amount of BMPR2 coimmunoprecipitated with Smurf1 (Fig. 7 G, compare lane 6 with lane 5), confirming that PINCH-1 inhibits the binding of BMPR2 to Smurf1. To test the effect of PINCH-1 on Smurf1-mediated degradation of BMPR2, we overexpressed either 3f-Smurf1 alone or 3f-Smurf1 together with 3f-P1 in MSCs. As expected, overexpression of 3f-Smurf1 reduced the level of BMPR2 (Fig. 7 H, lane 3). Overexpression of 3f-P1, however, completely reversed the reduction of BMPR2 level induced by overexpression of 3f-Smurf1 (Fig. 7 H, lane 4). Thus, the binding of PINCH-1 to Smurf1 effectively inhibits Smurf1-mediated binding (Fig. 7 K) and degradation of BMPR2.

The PINCH-1–Smurf1–BMPR2 signaling axis links mechano-environment to MSC fate decision

MSC fate decision is controlled to a great extent by mechano-environment. To test whether the PINCH-1–Smurf1–BMPR2 signaling axis identified in the foregoing experiments is involved in this process, we plated MSCs on ECM with different stiffness and analyzed the effects. PLA experiments showed that the level of the PINCH-1–Smurf1 complex in MSCs on soft ECM was markedly reduced compared with that in MSCs on stiff ECM (Fig. 7, I and J). Furthermore, PINCH-1 protein (Fig. 8 A, compare lane 1 with lane 3; and Fig. 8 B), but not mRNA (Fig. 8 C), level was significantly reduced in response to ECM softening, whereas the level of Smurf1 was not altered (Fig. 8 A). Consistent with a critical role of PINCH-1 in regulation of BMPR2 level, the protein (Fig. 8 A, compare lanes 1 and 3; and Fig. 8 B), but not mRNA (Fig. 8 C), level of BMPR2 was also reduced in response to ECM softening. Concomitant to the reduction of BMPR2 level, Smad1/5 phosphorylation was dramatically reduced (Fig. 8 A, compare lanes 1 and 3). The levels of Smad1 and kindlin-2 were not reduced in response to ECM softening (Fig. 8 A). To further investigate this, we tested the effects of ECM stiffness on the Smurf1–BMPR2 complex in MSCs. Human MSCs (hMSCs) expressing 3f-CA were used (Fig. 8 E), as a complex consisting of BMPR2 and catalytically active Smurf1 was barely detectable, presumably because BMPR2 was quickly degraded upon interaction with catalytically active Smurf1. As expected, the level of the 3f-CA–PINCH-1 complex was reduced in response to ECM softening (Fig. 8, D and F). Importantly, the level of the 3f-CA–BMPR2 complex was markedly increased in response to ECM softening (Fig. 8, D and G). Furthermore, overexpression of PINCH-1 in MSCs on soft ECM (Fig. 8 E, lane 4), which increased the level of the 3f-CA–PINCH-1 complex (Fig. 8, D and F), significantly reduced the level of the 3f-CA–BMPR2 complex (Fig. 8,

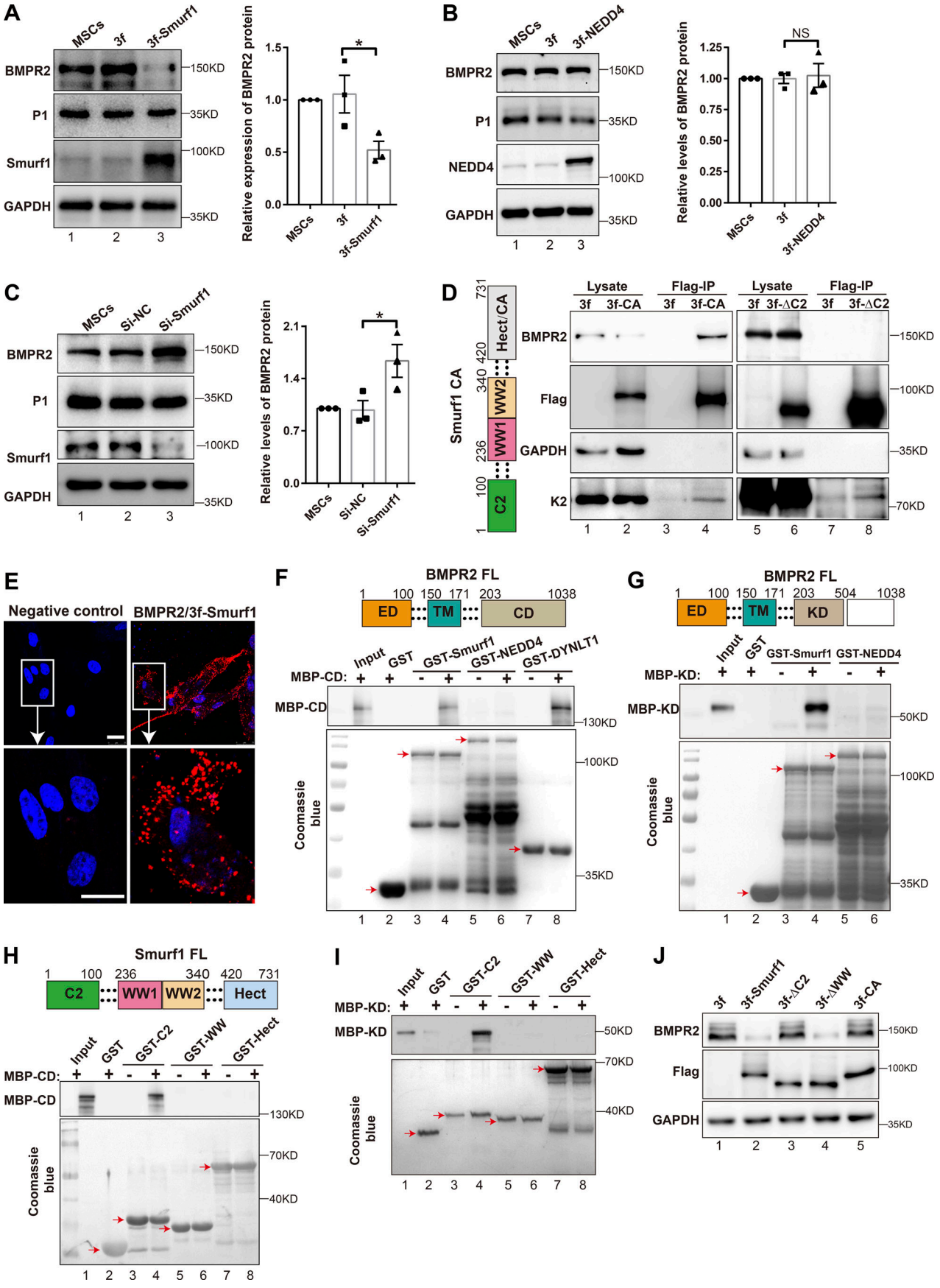

Figure 5. **Smurf1 interacts with BMPR2 via its C2 domain and mediates BMPR2 degradation. (A and B)** hMSCs were infected with 3f, 3f-Smurf1, or 3f-NEDD4 lentivirus for 3 d and analyzed by WB. Right: The levels of BMPR2 in infected hMSCs were quantified and compared with those in uninfected hMSCs (normalized to 1, $n = 3$). **(C)** hMSCs were transfected with Smurf1 siRNA (Si-Smurf1) or control siRNA (Si-NC) for 3 d and then analyzed by WB. Right: The levels of BMPR2 in transfectants were quantified and compared with those in untransfected hMSCs (normalized to 1, $n = 3$). **(D)** hMSCs were infected with 3f, 3f-CA, or 3f-ΔC2 lentivirus for 3 d and analyzed by coIP with an anti-FLAG Ab and WB with Abs recognizing FLAG, BMPR2, GAPDH, or kindlin-2 (K2). **(E)** hMSCs were infected with 3f or 3f-CA lentivirus for 3 d and then plated on soft collagen-I–coated hydrogels for 48 h. BMPR2 interaction with 3f-CA was analyzed by PLA. Scale bars = 25 µm. **(F–I)** His- and MBP-tagged BMPR2 CD (residues 203–1,038) or KD (residues 203–504) was incubated with GST, GST-Smurf1, various GST-Smurf1 mutants, GST-NEDD4, or GST-DYNLT1 as indicated and analyzed by GST pull-down assay. His- and MBP-tagged BMPR2 CD or KD was detected by WB with anti-His Ab. Bottom: The membranes were stained with Coomassie blue. Red arrows indicate the positions of GST or GST fusion proteins. **(J)** HEK293T cells were transfected with vectors encoding mCherry-BMPR2 and 3f-tagged WT or mutant forms of Smurf1 for 24 h and analyzed by WB. Data in A–C represent mean ± SEM. Statistical significance was calculated using one-way ANOVA with Tukey–Kramer post-hoc analysis, *P < 0.05; ED, extracellular domain; TM, transmembrane domain.

D and G). Consistent with this, overexpression of PINCH-1 in MSCs significantly increased BMPR2 level and downstream signaling despite being in contact with soft ECM (Fig. 8 A, compare lanes 3 and 4). Conversely, depletion of PINCH-1 in MSCs plated on stiff ECM, which reduced the level of the 3f-CA–PINCH-1 complex (Fig. 8, D and F), significantly increased the level of the 3f-CA–BMPR2 complex (Fig. 8, D and G). Consistent with a role of Smurf1 interaction in BMPR2 degradation, depletion of PINCH-1 significantly reduced BMPR2 level and downstream signaling despite the presence of stiff ECM (Fig. 8 A, compare lanes 1 and 2). Functionally, knockdown of PINCH-1 was sufficient to block OD and induce AD in MSCs, despite the fact that they were in contact with stiff ECM (Fig. 9, A–E). Conversely, overexpression of PINCH-1 (Fig. 9, A–E) or BMPR2 (Fig. 9, F–K) in MSCs on soft ECM was sufficient to induce OD and inhibit AD.

Inhibition of integrin internalization with MBCD reverses soft ECM–induced reduction of PINCH-1 level

We next sought to investigate the mechanism by which ECM stiffness regulates PINCH-1 level. Previous studies have shown that soft ECM enhances integrin internalization through caveolae/raft-dependent endocytosis (Du et al., 2011). Thus, we hypothesize that ECM stiffness may influence PINCH-1 level through alteration of caveolae/raft-dependent integrin internalization. To test this, we analyzed the levels of PINCH-1 in MSCs on ECM with different stiffness either in the presence or absence of methyl-β-cyclodextrin (MBCD), a caveolae/raft inhibitor that is known to suppress integrin internalization (Du et al., 2011). We confirmed that treatment with MBCD suppressed integrin internalization (Fig. 10 A). Importantly, suppression of integrin internalization with MBCD completely reversed the reduction of PINCH-1 level induced by soft ECM (Fig. 10 B). To further test this, we knocked down caveolin-1 and found that it also reversed soft ECM–induced reduction of PINCH-1 level (Fig. 10 C). Finally, soft ECM–induced reduction of PINCH-1 level was completely reversed by proteasome inhibitor MG132 or lysosomal inhibitor leupeptin (Fig. 10 D), suggesting that proteasome and lysosome are involved in soft ECM–induced down-regulation of PINCH-1 level.

Discussion

MSC fate decision is controlled to a great extent by mechano-environment (Vogel and Sheetz, 2009; Dupont et al., 2011; MacQueen et al., 2013; Chen et al., 2016; Vining and Mooney, 2017). Our studies presented in this report identify a novel signaling pathway consisting of PINCH-1, Smurf1, and BMPR2 that links mechano-environment to MSC fate decision. Specifically, we have found that the level of BMPR2, a key component of the BMP signaling pathway, is regulated by a mechano-responsive PINCH-1–Smurf1 complex. ECM stiffening increased the level of PINCH-1 and its complex formation with Smurf1, which, in turn, inhibited Smurf1 interaction with BMPR2 and thus blunted Smurf1-mediated BMPR2 degradation, resulting in elevation of BMPR2 level and consequently augmenting BMP signaling and MSC OD. Depletion of PINCH-1 was sufficient to inhibit BMP signaling and reprogram MSC fate from OD to AD, even in the presence of mechanical cues that favor OD (i.e., stiff ECM), suggesting that the PINCH-1–mediated signaling pathway is crucial for mechano-regulation of MSC fate decision. Furthermore, PINCH-1 deficiency–induced reprogramming of MSC fate (i.e., from OD to AD) can be effectively reversed by either depletion of Smurf1 or overexpression of BMPR2. Thus, PINCH-1 regulates MSC fate decision through, at least in part, control of Smurf1-mediated degradation of BMPR2. How does ECM stiffness influence the level of PINCH-1? Because ECM stiffening does not increase PINCH-1 mRNA level (Fig. 8 C), ECM stiffness likely regulates PINCH-1 at the protein level. Indeed, inhibition of proteasome with MG132 or lysosome with leupeptin markedly reversed soft ECM–induced reduction of PINCH-1 level (Fig. 10 D), suggesting that proteasome and lysosome are involved in this process. Previous studies have shown that ECM stiffness exerts a strong effect on integrin internalization through caveolae/raft-dependent endocytosis (Du et al., 2011). Consistent with the previous studies, treatment with caveolae/raft inhibitor MBCD inhibited integrin internalization (Fig. 10 A). Importantly, inhibition of integrin internalization completely blocked the reduction of PINCH-1 level induced by soft ECM (Fig. 10 B). Depletion of caveolin-1 also reversed soft ECM–induced down-regulation of PINCH-1 level (Fig. 10 C). Based on this and the previous studies (Du et al., 2011), we propose a model in which soft ECM promotes caveolae/raft-dependent integrin internalization, resulting in increased proteasome- and lysosome-mediated degradation of PINCH-1, which reduces the amount of PINCH-1 bound to Smurf1 and consequently increases Smurf1-mediated interaction/degradation of BMPR2 and suppresses BMP signaling and OD.

In addition to identifying the PINCH-1–Smurf1–BMPR2 axis as a key signaling pathway that mediates mechano-control of MSC differentiation, our studies have revealed important insights into the molecular mechanism through which PINCH-1

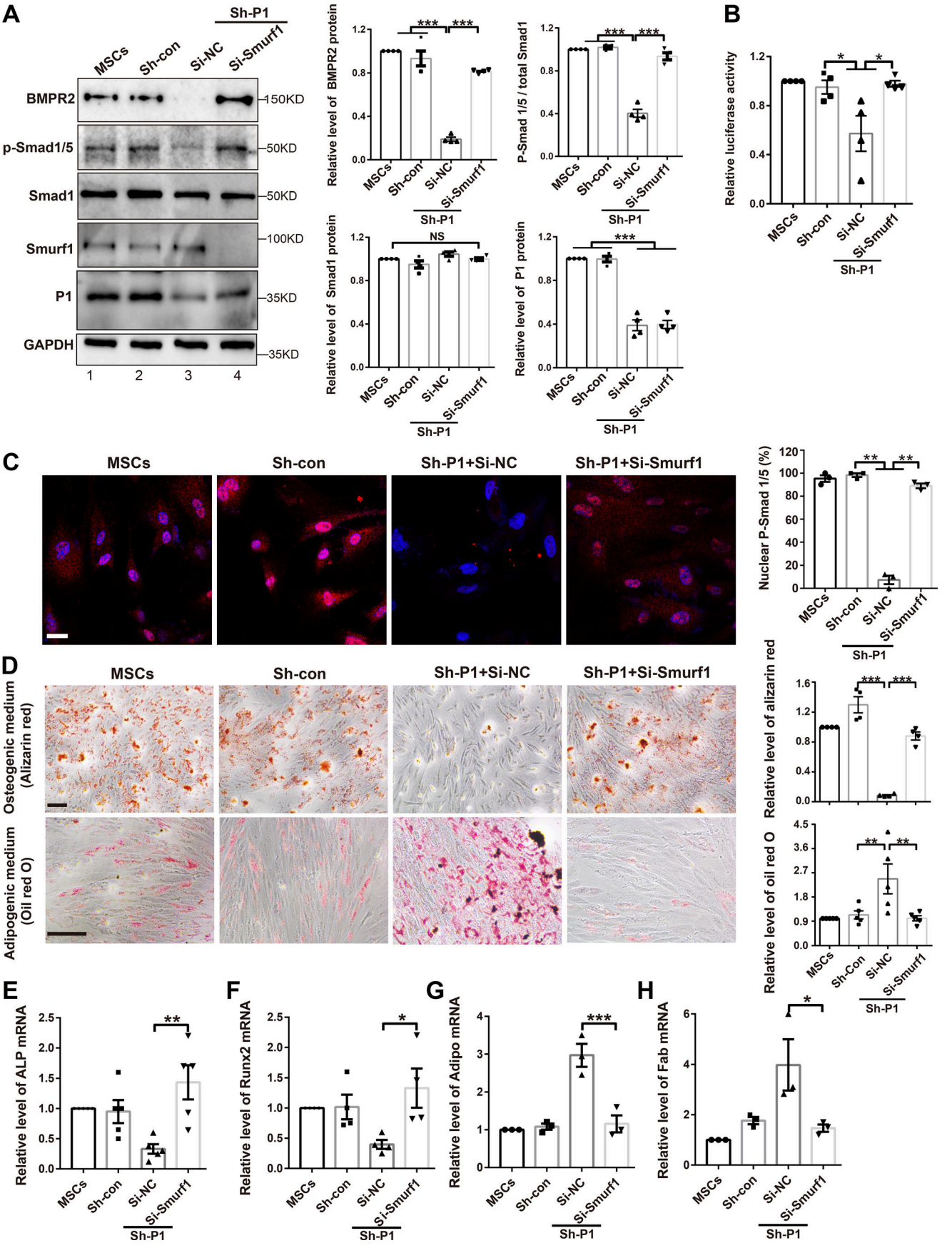

Figure 6. **Smurf1 is required for PINCH-1 regulation of BMPR2 expression and MSC differentiation. (A)** hMSCs were infected with Sh-P1 or Sh-con lentivirus for 2 d, transfected with Si-Smurf1 or Si-NC for 3 d, and analyzed by WB. Right: The protein levels in the infected hMSCs were quantified and compared with those in uninfected hMSCs (normalized to 1, $n \geq 3$). **(B)** hMSCs were infected with BRE-Luc lentivirus for 2 d and with Sh-P1 or Sh-con lentivirus for 2 d, and the Sh-P1 infectants were transfected with Si-Smurf1 or Si-NC for 2 d. BMP reporter activities were assessed by measuring luciferase activity in the infected cells and comparing that with the reporter cells that were not infected with Sh-P1 or Sh-con (normalized to 1, $n = 4$). **(C)** Cells treated as above (A) were immunofluorescently stained with DAPI and Abs for p-Smad1/5. Scale bar = 25 µm. Right: The percentages of nuclear p-Smad1/5–positive cells among total cells were quantified ($n = 3$). **(D)** The cells were cultured in OD or AD medium for 14 d and stained with Alizarin red S or oil red O as indicated. Scale bars = 100 µm. Right: Alizarin red S– or oil red O–positive areas in the infectants were quantified and compared with those in uninfected MSCs (normalized to 1, $n \geq 4$). **(E–H)** The mRNA levels of ALP and Runx2 (E and F) and Adipo and Fab (G and H) in the infected MSCs were analyzed by RT-PCR and compared with those of uninfected MSCs (normalized to 1, $n \geq 3$). Data are presented as mean ± SEM using one-way ANOVA with Tukey–Kramer post-hoc analysis, *P < 0.05; **P < 0.01; ***P < 0.001.

regulates Smurf1 binding and degradation of BMPR2. Smurf1, which was originally identified based on its interaction with Smad1 and targeting it for degradation (Zhu et al., 1999), contains a C2 domain in its N-terminus, two WW domains in the middle, and a catalytic HECT domain in its C-terminus. Smurf1 can interact not only with R-Smads (e.g., Smad1 and 5), but also with other proteins, including Runx2, RhoA, ARHGEF9/hPEM2, BMPR1A, MEKK2, Talin head, Prickle1, kindlin-2, STAT1, KLF2, WFS1, and ING2 (Zhu et al., 1999; Kavsak et al., 2000; Podos et al., 2001; Murakami et al., 2003; Wang et al., 2003; Ying et al., 2003; Zhao et al., 2003; Yamashita et al., 2005; Yamaguchi et al., 2008; Huang et al., 2009; Narimatsu et al., 2009; Nie et al., 2010; Guo et al., 2011; Xie et al., 2011; Yuan et al., 2012; Cao and Zhang, 2013; Wei et al., 2017). Through interacting and targeting different substrates for degradation, Smurf1 regulates a variety of cellular processes including cell differentiation, proliferation, polarity, adhesion, migration, DNA damage response, and immune responses (Cao and Zhang, 2013). Therefore, determining the molecular basis underlying specific Smurf1–substrate interactions, as well as their regulatory mechanisms, is important for understanding the mechanisms whereby Smurf1 functions in these diverse cellular processes. In this study, we have found that the interaction with BMPR2 is mediated by Smurf1 C2 domain (Fig. 5). Importantly, PINCH-1 also interacts with the C2 domain, and PINCH-1 interaction inhibits Smurf1 binding and degradation of BMPR2 (Fig. 7). These findings provide an explanation as to why overexpression of PINCH-1 inhibited the Smurf1–BMPR2 complex and increased BMPR2 level in MSCs (Figs. 7 and 8). Furthermore, they also explain why knockdown of PINCH-1 increased the Smurf1–BMPR2 complex and reduced BMPR2 level in MSCs (Figs. 3 and 8). It is interesting to note that the levels of Smad1 and BMPR1A were not altered by knockdown or overexpression of PINCH-1 (Fig. 3). This is consistent with the fact that Smad1 and BMPR1A bind to Smurf1 WW or HECT, but not C2 domain (Aragón et al., 2011; Chaikuad and Bullock, 2016), which is the primary binding target of PINCH-1 (Fig. 7).

While the findings presented in this paper clearly demonstrate that PINCH-1 acts as a key regulator of BMP signaling and MSC differentiation in response to mechanical signals, other proteins and signaling pathways also contribute to mechano-regulation of MSC differentiation. For example, we recently found that kindlin-2 is also involved in mechano-regulation of MSC differentiation (Guo et al., 2018). However, depletion of kindlin-2, unlike that of PINCH-1, did not significantly reduce the level of BMPR2 (Fig. S1 B), suggesting that the mechanism by which kindlin-2 regulates MSC differentiation differs from that of PINCH-1, which is consistent with our previous studies showing that kindlin-2 mediates mechano-regulation of MSC differentiation through control of YAP1/TAZ expression and signaling (Guo et al., 2018). Thus, it is likely that multiple signaling pathways, including those consisting of PINCH-1–Smurf1–BMPR2 (the current study) or kindlin-2–YAP1/TAZ (Guo et al., 2018), are involved in mechano-regulation of MSC differentiation. Interestingly, knockdown of ILK, a PINCH-1–binding protein (Tu et al., 1999; Zhang et al., 2002), did not significantly reduce the level of BMPR2 (Fig. S1 A), suggesting that ILK probably does not play a direct role in PINCH-1–mediated interaction with Smurf1 and inhibition of BMPR2 degradation. This is consistent with the fact that PINCH-1 is capable of interacting with Smurf1 or its C2 domain and inhibiting Smurf1 interaction with BMPR2 in the absence of ILK (Fig. 7, C–F). Thus, while complex formation with ILK is critical for many PINCH-1–mediated functions, as previously shown by us and others (Tu et al., 1999; Wu and Dedhar, 2001; Guo and Wu, 2002; Zhang et al., 2002; Fukuda et al., 2003; Wu, 2004, 2005; Yang et al., 2005; Li et al., 2007; Wickström et al., 2010; Rooney and Streuli, 2011; Qin and Wu, 2012), it is likely that not all functions of PINCH-1 are dependent on ILK. Furthermore, while ILK does not seem to play a major role in PINCH-1–mediated interaction with Smurf1 and inhibition of BMPR2 degradation, the studies presented in this paper did not test the role of ILK in mechano-regulation of MSC differentiation and therefore do not rule out the possibility that ILK may contribute to this process through other mechanisms.

Although the studies presented in this report focus on the mechanism of the PINCH-1–Smurf1–BMPR2 signaling pathway and its function in mechano-regulation of MSC differentiation, the PINCH-1–Smurf1–BMPR2 signaling pathway identified in the current study may also function in other physiological and pathological processes involving Smurf1 and BMPR2. In this regard, it is particularly interesting to note that mutations in the *BMPR2* gene are linked to the development of human pulmonary arterial hypertension (PAH; Deng et al., 2000; Lane et al., 2000). It was estimated that ∼80% of patients with familial PAH and 20% of patients with idiopathic PAH bear heterozygous *BMPR2* mutations (Deng et al., 2000; Aldred et al., 2006; Cogan et al., 2006). Numerous studies have shown that BMPR2 deficiency is a major causal factor in the pathogenesis of PAH (Atkinson et al., 2002; Orriols et al., 2017; Andruska and Spiekerkoetter, 2018). However, because the penetrance of *BMPR2* mutations is only

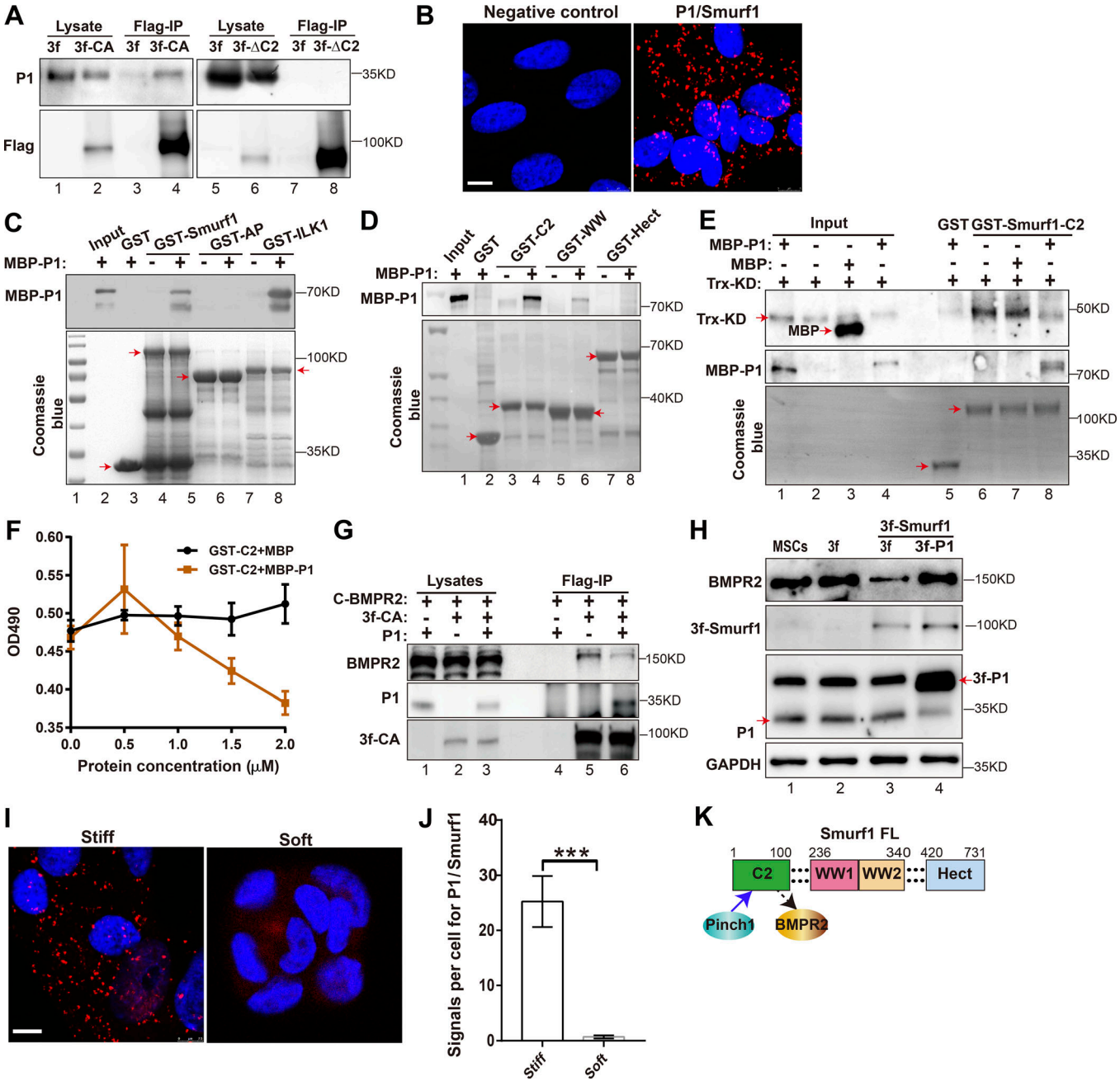

Figure 7. **PINCH-1 interacts with Smurf1 C2 domain and inhibits Smurf1-mediated binding and degradation of BMPR2. (A)** hMSCs were infected with 3f, 3f-CA, or 3f-ΔC2 lentivirus for 3 d and analyzed by IP and WB. **(B)** hMSCs were plated on stiff collagen-I–coated hydrogels for 48 h and analyzed by PLA with Abs for PINCH-1 and Smurf1 Abs. Scale bar = 8 µm. **(C and D)** His- and MBP-tagged PINCH-1 (MBP-P1) was incubated with GST, GST-Smurf1, or GST-tagged Smurf1 mutants and analyzed by GST pull-down assay. Top: PINCH-1 was detected by WB with anti-His Ab. Bottom: The membranes were stained with Coomassie blue. Red arrows indicate the positions of GST and GST fusion proteins. **(E)** GST and GST-Smurf1 C2 bound to glutathione resins were preincubated with MBP-his or MBP-his–PINCH-1 as indicated and then used to pull down Trx-His–BMPR2 KD. Trx-His–BMPR2 KD (top) and MBP-his–PINCH-1 (middle) were detected by WB with an anti-His Ab. Bottom: The membrane was stained with Coomassie blue. Red arrows indicate the positions of GST and GST-Smurf1 C2. **(F)** PINCH-1 inhibition of the interaction between Smurf1 C2 and BMPR2 KD was analyzed using an ELISA-based binding assay. The data are expressed as mean ± SEM of triplicates from a representative experiment. OD490, optical density of 490. **(G)** HEK293T cells were transfected with pLVX vectors encoding Cherry-BMPR2, 3f-CA, and/or PINCH-1 for 24 h and analyzed by IP and WB. **(H)** hMSCs were infected with 3f or 3f-Smurf1 lentivirus for 2 d, and then the 3f-Smurf1 infectants were infected with 3f-P1 lentivirus. 3 d later, the cells were analyzed by WB. **(I and J)** hMSCs were plated on stiff or soft collagen-I–coated hydrogels for 48 h and analyzed by PLA with Abs for PINCH-1 and Smurf1 Abs. **(I)** The nuclei were stained with DAPI. The signals of PLA (red) and DAPI staining (blue) were visualized under fluorescent microscopy. Scale bar = 8 µm. **(J)** The number of PLA dots per cell was calculated. The data are presented as mean ± SEM using Student's *t* test (two tailed), ***P < 0.001. **(K)** Schematic diagram depicts a model showing that PINCH-1 competitively inhibits the interaction of Smurf1 C2 with BMPR2.

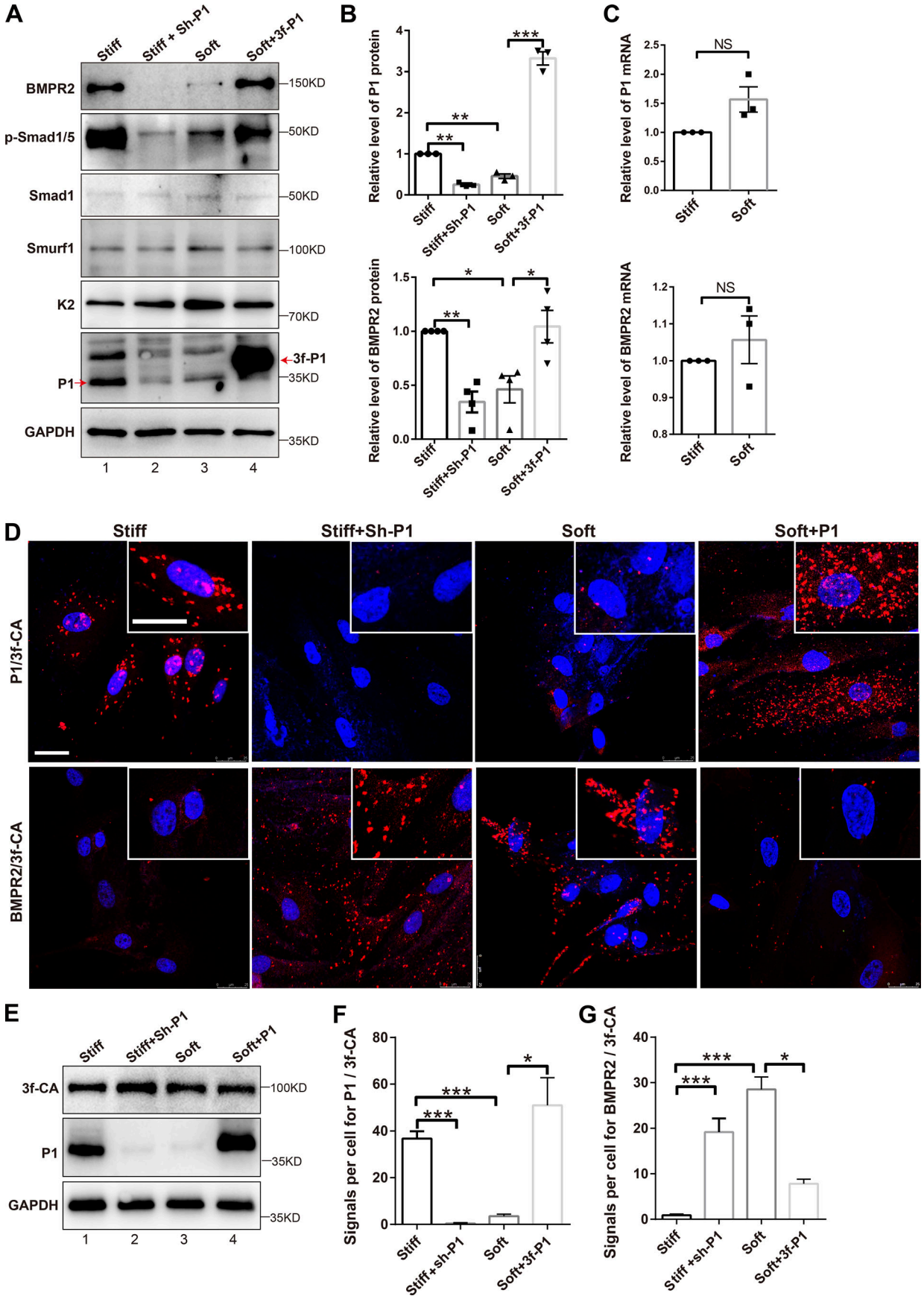

Figure 8. **The PINCH-1–Smurf1–BMPR2 axis mediates mechano-control of MSC differentiation. (A)** hMSCs were infected with Sh-P1 or 3f-P1 for 3 d, plated on stiff or soft collagen-I–coated hydrogels for 48 h, and analyzed by WB. Red arrows indicate the positions of P1 or 3f-P1. **(B)** The P1 and BMPR2 protein levels in P1 knockdown hMSCs on stiff ECM, control hMSCs on soft ECM, and P1-overexpressing hMSCs on soft ECM were quantified by densitometry and compared with those of control hMSCs on stiff ECM (normalized to 1, $n = 3$). **(C)** The mRNA levels of P1 and BMPR2 in hMSCs on soft ECM were analyzed by RT-PCR and compared with those in hMSCs on stiff ECM (normalized to 1, $n = 3$). **(D–G)** hMSCs expressing 3f-CA were infected with lentiviral vectors encoding P1 or Sh-P1 for 3 d, plated on stiff or soft collagen-I–coated hydrogels for 48 h, and analyzed by PLA with Abs for P1, BMPR2, or FLAG as indicated. **(D)** The nuclei were stained with DAPI. PLA signals (red) and DAPI staining (blue) were visualized under fluorescent microscopy. Scale bars = 25 µm. **(E)** The cells were analyzed by WB. **(F and G)** The numbers of PLA dots per cell were counted. Data in B, F, and G are presented as mean ± SEM using one-way ANOVA with Tukey–Kramer post-hoc analysis, and data in C were analyzed using Student's *t* test (two tailed), *P < 0.05; **P < 0.01; ***P < 0.001.

~20% (Newman et al., 2004), mechanisms other than *BMPR2* mutations must exist that can also cause BMPR2 deficiency in PAH. Recent studies have suggested an important role of Smurf1 in BMPR2 degradation and pathogenesis of PAH (Murakami et al., 2010; Rothman et al., 2016). Thus, because PINCH-1 plays a key role in regulation of Smurf1-mediated binding and degradation of BMPR2 (the current study), it will be interesting to investigate in future studies whether PINCH-1 is involved in the pathogenesis of at least a subpopulation of PAH patients (e.g., those with reduced BMPR2 level but lacking BMPR2 mutations).

Materials and methods

DNA constructs, lentivirus production, and infection

The pLKO.1-TRC, psPAX2, and pMD2.G vectors were obtained from Addgene (plasmid #10878, plasmid #12260, and plasmid #12259). The pLKO.1 vectors expressing shRNAs targeting human PINCH-1 (Sh-PINCH-1) or scrambled shRNA (Sh-con) sequence were generated using the following sequences: Sh-PINCH-1, 5′-AAGGTGATGTGGTCTCTGCTC-3′; and Sh-con, 5′-ACGCATGCA TGCTTGCTTT-3′. To generate lentiviruses encoding the above shRNAs, HEK293T cells were co-transfected with pLKO.1 encoding the various shRNAs and lentiviral constructs (psPAX2 and pMD2.G). The expression vectors encoding human PINCH-1, BMPR2, Smurf1-CA, Smurf1-ΔC2, or BRE-Luc (pLVX-PINCH-1, pLVX-BMPR2, pLVX-Smurf1-CA, pLVX-Smurf1-ΔC2, or pLVX-BRE-Luc) were generated by cloning the corresponding cDNA sequences into the pLVX-IRES-hyg vector (Clotech). The sequence corresponding to the shRNA targeting region in the PINCH-1 expression vectors was changed to 5′-AAGGCGACGTCGTGTCTG CTC-3′ to confer resistance to the PINCH-1 shRNA (Sh-P1). The sequences of all DNA inserts were verified by DNA sequencing (Invitrogen). To generate lentiviruses, vectors encoding human pLVX-PINCH-1, pLVX-BMPR2, pLVX-Smurf1-CA, or pLVX-BRE-Luc were co-transfected with psPAX2 and pMD2.G into HEK293T cells. After the cells were incubated at 37°C and 5% CO_2 for 24–48 h, the media containing lentiviral particles were harvested. For lentiviral infection, hMSCs were cultured in basal growth medium until 70% confluence and then replaced with fresh medium containing lentivirus at an MOI of 100 for 16 h. Lentiviral infections were performed in the presence of 8 µg ml^{-1} polybrene.

GST pull-down assays

For preparation of GST fusion proteins containing WT or mutant forms of Smurf1, the corresponding cDNA sequences were cloned into pGEX-4T-1 vector, which were transfected into *Escherichia coli* Bl21. GST and GST fusion proteins were purified with Glutathione–Sepharose 4B matrix (GE Healthcare) following the manufacturer's instructions. MBP-his–tagged PINCH-1 and WT or mutant forms of BMPR2 were expressed in *E. coli* and purified by affinity chromatography with amylose resin (Biolabs, #E8021S). Purified proteins were resolved by SDS-PAGE to verify their sizes and purity. For GST pull-down assays, GST or GST fusion proteins bound to Glutathione-Sepharose beads were incubated with MBP-his–tagged PINCH-1 and WT or mutant forms of BMPR2 for 2 h at 4°C. The beads were washed three times with buffer (20 mM Tris, pH 7.5, 150 mM NaCl, and 0.1% Triton X-100) and then analyzed by SDS-PAGE and WB with antibodies (Abs) as specified in each experiment.

RNA interference

siRNA directed against human Smurf1 or caveolin-1 was synthesized by Invitrogen. The sense sequences of siRNAs were as follows: Smurf1 siRNA, 5′-GCAGCUGCUAGAUAUCUUATT-3′; caveolin-1 siRNA, 5′-GCAUUUGGAAGGCCAGCUUTT-3′; and control siRNA (Si-NC), 5′-ACGCATGCATGCTTGCTTT-3′. Transfection of siRNAs to hMSCs was performed using Lipofectamine RNAiMAX Reagent (Life Technologies). Cells were transfected with 25 pmol per 6-well culture dish (1×10^5 cells per milliliter in 6-well plates).

Cell isolation and culture

hMSCs were isolated from human placenta as previously described (Guo et al., 2014; Wang et al., 2015). hMSCs were seeded on cell culture dishes with a growth medium consisting of DMEM (Gibco-Invitrogen), 10% FBS (Gibco-Invitrogen), and antibiotics. In some experiments, hMSCs (as specified in each experiment) were cultured in the presence of proteasome inhibitor MG-132 (10 µM), lysosomal inhibitor leupeptin (10 µM), or caveolae/raft inhibitor MBCD (10 mM) for 24 h before further analyses.

Preparation of collagen-coated polyacrylamide hydrogels with different stiffness

Preparation of collagen-coated polyacrylamide hydrogels with different stiffness was performed as previously described (Wang and Pelham, 1998; Cretu et al., 2010). Briefly, glass coverslips were activated successively with 100 mM NaOH for 5 min, 3-aminopropyltri-methoxysilane (Sigma-Aldrich, #281778) for 5 min, and 0.5% glutaraldehyde (Sigma-Aldrich, #G7776) for 30 min. Hydrogels with different stiffness (soft vs. stiff) were prepared with two prepolymer solutions containing different acrylamide/bis-acrylamide ratios. The elastic moduli of stiff and

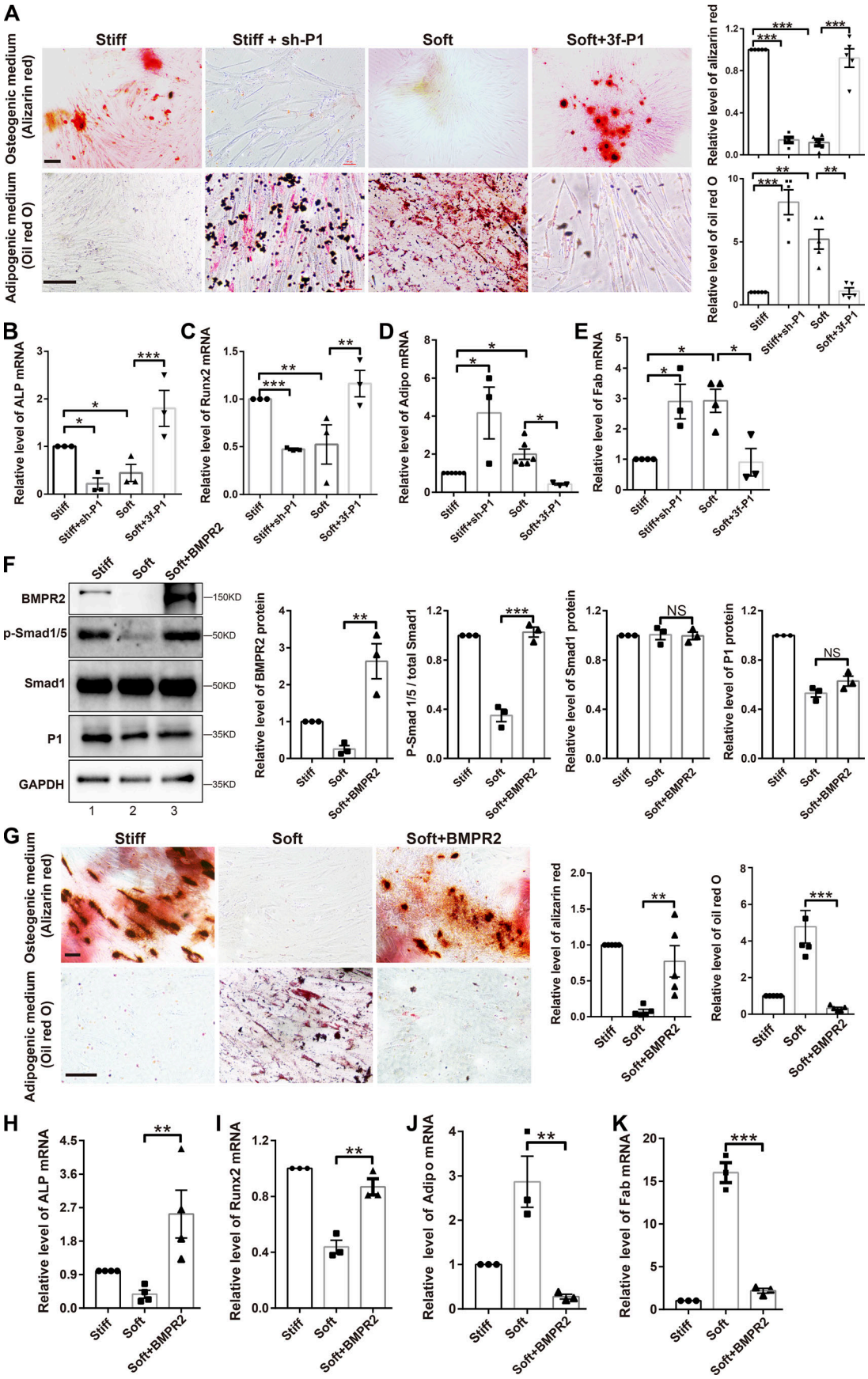

Figure 9. **PINCH-1 and BMPR2 mediate ECM stiffening–induced MSC OD. (A)** hMSCs were infected with 3f-P1 or Sh-P1 lentivirus for 3 d, plated on stiff or soft collagen-I–coated hydrogels, cultured in growth medium for 48 h and then in OD or AD medium for 8 d, and stained with Alizarin red S or oil red O. Scale bars = 100 µm. Right: Alizarin red S– or oil red O–positive areas in the cells (as indicated) were quantified and compared with those in uninfected hMSCs on stiff ECM (normalized to 1). **(B–E)** The mRNA levels of ALP and Runx2 (B and C) and Adipo and Fab (D and E) in the cells (as indicated) were analyzed by RT-PCR and compared with those in uninfected hMSCs on stiff ECM (normalized to 1, *n* = 3). **(F)** hMSCs were infected with 3f-BMPR2 lentivirus. 3 d after infection, hMSCs, with or without BMPR2 overexpression, were plated on stiff or soft collagen-I–coated hydrogels, cultured in growth medium for 48 h, and analyzed by WB. Right: The protein levels in uninfected hMSCs on soft ECM and BMPR2-overexpressing hMSCs on soft ECM were quantified and compared with those of uninfected hMSCs on stiff ECM (normalized to 1, *n* = 3). **(G)** hMSCs, with or without BMPR2 overexpression, were plated on stiff or soft collagen-I–coated hydrogels, cultured in growth medium for 48 h, and then cultured in OD or AD medium for 8 d. The cells were stained with Alizarin red S or oil red O. Scale bars = 100 µm. Right: Alizarin red S– or oil red O–positive areas in the cells (as indicated) were quantified and compared with those in uninfected hMSCs on stiff ECM (normalized to 1, *n* = 5). **(H–K)** The mRNA levels of ALP and Runx2 (H and I) and Adipo and Fab (J and K) in the cells were analyzed by RT-PCR and compared with those in uninfected hMSCs on stiff ECM (normalized to 1, *n* = 3). Data are presented as mean ± SEM using one-way ANOVA with Tukey–Kramer post-hoc analysis, *P < 0.05; **P < 0.01; ***P < 0.001.

soft hydrogels were ∼40 kPa and 0.35 kPa, respectively. The polyacrylamide sheets were assembled on the activated coverslips upon the addition of 0.5% ammonium persulfate (Sigma-Aldrich, #09830) and 0.005% tetramethylethylenediamine and subsequently activated by incubation with 1 mM Sulfo-SANPAH (Thermo Scientific, #22589) under 452-nm UV light for 5 min. The activated polyacrylamide sheets were then coated with 0.3 mg ml^{-1} collagen-I at 4°C overnight. hMSCs were cultured on collagen-I–coated gels (1.5 × 10^5 cells per 3.0-cm-diameter coverslip) and analyzed as specified in each experiment.

MSC differentiation in culture

hMSCs were cultured in various media as specified in each experiment. For induction of AD, hMSCs were cultured in DMEM supplemented with 10% FBS, 1% penicillin-streptomycin, 125 µM 3-isobutyl-1-methylxanthine (Sigma-Aldrich), 0.25 µM dexamethasone (Sigma-Aldrich), 2.5 µM insulin (Sigma-Aldrich), and 50 µM indomethacin (Sigma-Aldrich). 14 d later, cells were fixed in 4% paraformaldehyde and stained with oil red O (Sigma-Aldrich) until obvious signals were detected in one or more of the cell groups (e.g., sh-P1 cell group; Guo et al., 2014). The cells were then rinsed three times with PBS to stop the staining. For induction of OD, hMSCs were cultured in DMEM–high glucose supplemented with 10% FBS, 1% penicillin-streptomycin, 10 nM dexamethasone, 50 µM ascorbic acid 2-phosphate (Sigma-Aldrich), and 10 mM β-glycerophosphate (Sigma-Aldrich). 14 d later, cells were fixed in 4% paraformaldehyde and stained with Alizarin red S (Sigma-Aldrich) to observe mineralized matrix deposition (Wu et al., 2007; Li et al., 2011; Guo et al., 2014). Images were acquired at room temperature using a microscope (Eclipse TS100; Nikon) with long working distance 10×/0.25 and long working distance 20×/0.4 objectives (Nikon) equipped with a digital camera (TS100-F; Nikon) and NIS-Elements F version 4.00.00 (Nikon) image software. Alizarin red S and oil red O staining were quantified from four to five microscopic fields using ImageJ.

MSC differentiation in vivo

GFP-labeled hMSCs (2 × 10^6 per milliliter) that were infected with Sh-P1 or Sh-con lentivirus were embedded into matrix gels as previously described (Guo et al., 2018). hMSCs in matrix gels were induced with OD medium for 3 d. The matrix plugs were then implanted subcutaneously into Nu/Nu mice. The specimens were dissected from the mouse recipients and analyzed 10 d later by H&E staining, WB, and anti-ALP and anti-perilipin immunofluorescent (IF) staining as described in Tang et al. (2013).

Quantitative real-time PCR analysis

cDNA was synthesized from 10 ng total RNA using the ReverTra Ace qPCR RT Master Mix (Toyobo Life Science) according to the manufacturer's protocol. Real-time PCR was performed in a 20-µl reaction volume using SYBR Green Realtime PCR Master Mix (Toyobo Life Science) on an ABI 7500 QPCR System. As an internal control, levels of GAPDH mRNA were quantified in parallel with mRNAs of the target genes. Normalization and fold changes were calculated using the ΔΔCt method. Primer sets are listed in Table S1.

WB

WB was performed as previously described (Wu et al., 2015). For preparation of whole cell protein lysates, cells were lysed in 1% SDS lysis buffer (25 mM Tris-HCl, pH 6.8, 50 mM DTT, 10% glycerin, and 2.5% sucrose). Equal amounts (10–60 µg/lane) of total protein were separated on 10% polyacrylamide gel and transferred onto a nitrocellulose membrane. Membranes were blocked for 1 h at room temperature in TBS (50 mM Tris-HCl and 150 mM NaCl, pH 7.4) containing 0.1% Tween 20 and 5% nonfat powdered milk, followed by overnight incubation at 4°C with HRP-conjugated mouse anti-GAPDH (Santa Cruz, sc-47724 HRP), HRP-conjugated mouse anti–FLAG-M2 HRP (Sigma-Aldrich, A8592 HRP), rabbit anti–PINCH-1 (Proteintech, 20772–1-AP), rabbit anti-BMPR2 (Cell Signaling, 6979S), rabbit anti-BMPR1A (Proteintech, 12702–1-AP), rabbit anti–p-Smad1/5 (Cell Signaling, 9516S), rabbit anti-Smad1 (Cell Signaling, 9743S), rabbit anti–caveolin-1 (Cell Signaling, 3238S), mouse anti-Smurf1 (Santa Cruz, sc-100616), or mouse anti-His (Tiangen, AB102-02) Abs. After washing and incubation with appropriate HRP-conjugated secondary anti-rabbit or mouse IgG Abs (Jackson ImmunoResearch, #711-005-152 or #715-005-151), the blots were developed using an ECL kit (Bio-Rad) or the Ultra ECL Western Blotting Detection Reagent (4A Biotech, 4AW011) and then exposed using an automatic digital gel image analysis system (Tanon, 6100B) or x-ray film (Fujifilm, # super RX-N-C). The images were scanned using an imaging scanning system (EPSON Scan L365) and quantified with ImageJ. The levels of BMPR2, BMPR1A, Smad1, and PINCH-1 relative to GAPDH, and that of p-Smad1/5

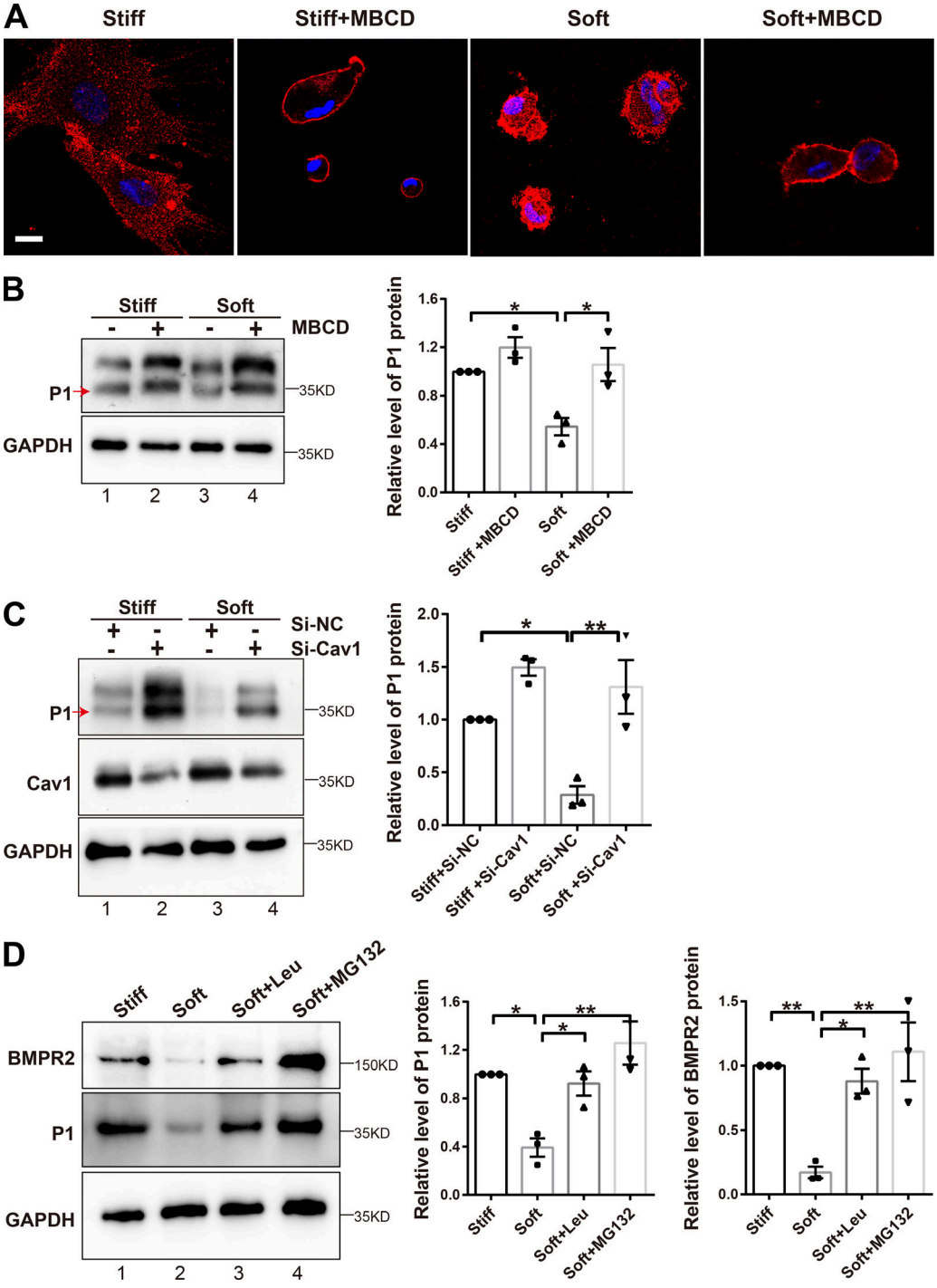

Figure 10. **Inhibition of caveolae/raft-dependent integrin internalization with MBCD or depletion of caveolin-1 reverses soft ECM–induced down-regulation of PINCH-1 level. (A and B)** hMSCs on stiff and soft collagen-I–coated hydrogels were treated with or without 10 mM MBCD for 24 h, stained with an anti–β1 integrin Ab (A), and analyzed by WB (B). Scale bar = 25 µm. **(B)** Right: P1 levels in the samples (as indicated) were quantified and compared with those of untreated hMSCs on stiff ECM (normalized to 1, *n* = 3). **(C)** hMSCs were transfected with caveolin-1 siRNA (Si-Cav1) or Si-NC for 2 d, plated on stiff or soft collagen-I–coated hydrogels for 48 h, and analyzed by WB. Right: P1 levels in the samples (as indicated) were quantified and compared with those in Si-NC cells on stiff ECM (normalized to 1, *n* = 3). **(D)** hMSCs on stiff and soft hydrogels were treated with or without MG132 (10 µM) or with leupeptin (10 µM) for 24 h and analyzed by WB. Right: P1 and BMPR2 levels in the samples (as indicated) were quantified and compared with those in untreated hMSCs on stiff ECM (normalized to 1, *n* = 3). Data are presented as mean ± SEM using one-way ANOVA with Tukey–Kramer post-hoc analysis, *P < 0.05; **P < 0.01. Red arrows indicate the position of P1.

relative to total Smad1, were calculated by quantification of the data from at least three independent experiments.

Immunofluorescence

hMSCs (2×10^4 per well) were seeded on coverslips in 24-well plates and cultured overnight. The cells were then immersed in 0.1% Triton X-100 in PBS for 10 min at room temperature, followed by washing three times with PBS. The cells were incubated with rabbit anti-ALP (Genetex, #GTX62596), rabbit anti-perilipin (Cell Signaling, 9391S), or mouse anti–p-Smad1/5 (Cell Signaling, 9516S) Abs at 4°C overnight. The cells were then washed with PBS and incubated with Alexa Fluor 594/488–conjugated anti-mouse or rabbit (Invitrogen) secondary Abs (1:300) for 1 h at room temperature. Images were acquired at 21°C using an SP8 confocal fluorescence microscope (63× oil objective, 1.4 NA; Leica) with Leica X version 1.1.0.12420 image software. Anti-ALP and anti-perilipin IF staining were quantified from five microscopic fields using ImageJ. The percentages of cells with positive nuclear p-Smad1/5 staining among total cells were calculated. At least 50 cells were analyzed in each experiment.

IP

hMSCs infected with FLAG-Smurf1-CA were harvested and homogenized in WB and IP lysis buffer (Beyotime Biotechnology, P0013) supplemented with 1 mM PMSF (Sigma-Aldrich, #329–98-6) for 30 min at 4°C. IP was performed by mixing an equal amount of cell lysates (2–3 mg protein) with an equal amount of anti-FLAG M2-conjugated agarose beads (10–30 µl of 50% suspension; Sigma-Aldrich, A2220) and incubated for 2 h. The IP samples were washed once with the lysis buffer and twice with PBS. The samples were then analyzed by WB with rabbit anti-BMPR2 (Cell Signaling, 6979S), rabbit anti–PINCH-1 (Proteintech, 20772–1-AP), or mouse anti-FLAG (Sigma-Aldrich, F1804) Abs.

PLA

PLA was performed on fixed hMSCs with Duolink PLA technology probes and reagents (Sigma-Aldrich) following the manufacturer's instructions. Briefly, cells (as specified in each experiment) were permeabilized with PBS containing 0.5% Triton X-100 for 15 min. After washing with PBS twice, the cells were incubated with blocking solution for 30 min at 37°C and then incubated with pairs of rabbit and mouse Abs as specified in each experiment (e.g., pairs of rabbit anti-BMPR2 [Proteintech, 19087–1-AP] and mouse anti-FLAG [Sigma-Aldrich, F1804], mouse anti–PINCH-1 [BD Biosciences, 612711] and rabbit anti-Smurf1 [Proteintech, 55175–1-AP], or mouse anti–PINCH-1 [BD Biosciences, 612711] and rabbit anti-FLAG [Proteintech, 20543–1-AP]). The cells were incubated with the Abs at 4°C overnight. The coverslips were washed three times with buffer A provided by the manufacturer for 5 min, followed by incubation with the PLA probes (secondary Abs against the primary Abs from different species bound to two oligonucleotides; e.g., anti-mouse MINUS and anti-rabbit PLUS) in Ab diluent for 60 min at 37°C. After washing three times with buffer A for 5 min, the ligation step was performed with ligase diluted in the ligation buffer for 30 min at 37°C. In the ligation step, the two oligonucleotides in the PLA probes were hybridized to the circularization oligonucleotides. The cells were washed twice with buffer A for 5 min, followed by incubation with amplification solution at 37°C for 100 min. The amplification solution contains polymerase for the rolling circle amplification step and oligonucleotides labeled with fluorophores, which binds to the product of the rolling circle amplification and thus allows detection. After washing twice with buffer B provided by the manufacturer for 10 min and once with 0.01× buffer B for 1 min, the coverslips were mounted with Duolink in situ mounting medium containing DAPI. For every experiment, a negative control was included in which one of the two Abs was replaced with control IgG from the same species. In addition, a pair of rabbit anti–Ki-67 (CST, #12202) and mouse anti-Smurf1 (Abcam, ab57573) Abs was used as an additional negative control, and a pair of mouse anti–kindlin-2 (3A3.5) and rabbit anti-Smurf1 (Proteintech, 55175–1-AP) Abs was used as a positive control. At least 20 cells were analyzed for each experiment. All experiments were repeated at least three times.

Integrin internalization

Integrin internalization assay was performed based on the method described by Du et al. (2011) with minor modifications. Briefly, hMSCs grown on soft substrate were treated with or without 10 mM MBCD for 24 h. The cells were then incubated with an Ab for β1 integrin (1:300; Millipore, #MAB1987) at 4°C for 45 min. After washing three times, cells were incubated at 37°C for 30 min to allow integrin internalization. At the end of the incubation, cell surface Abs were removed with acidic medium (pH 4.0). Internalized β1 integrin bound to the Ab was detected with FITC-conjugated anti-mouse IgG Abs (1:1,000; Abcam).

ELISA-based direct binding assay

Stripwell plates (Corning) were coated with 1 µM Trx-His-BMPR2 KD in 50 mM carbonate buffer (pH 9.6) overnight at 4°C. 1.5 µM BSA (VWR Life Science) and 1.5 µM GST-Smurf1-C2 diluted in the same buffer were used as negative and positive controls, respectively. Plates were washed three times with PBS and then blocked with 1% BSA. After washing three more times with PBS, the samples of 1.5 µM GST-Smurf1-C2 containing 0.1% BSA and increasing concentrations of MBP or MBP–PINCH-1 (as specified in each experiment) were applied to wells and incubated at 37°C for 1 h. The wells were washed three times with PBS. HRP-conjugated anti-GST-Tag Ab (Proteintech, HRP-66001) and HRP detection reagent (Cytoskeleton) were used to detect GST-Smurf1-C2 bound to immobilized Trx-His-BMPR2 KD. An optical density of 490 was determined using an Epoch2 (BioTek) microplate reader.

BMP reporter assay

hMSCs were infected with BRE-Luc reporter lentivirus containing BREs from the Id1 promoter fused to a luciferase reporter gene (Korchynskyi and ten Dijke, 2002; Yadav et al., 2012). 2 d later, the reporter cells were infected with various lentiviral vectors as specified in each experiment. To measure luciferase activities, the cells were harvested, suspended in culture medium, and added to wells (100 µl containing 10^4 cells/well) of 96-well white wall plates. The plates were incubated at 37°C in a

humidified cell culture incubator with 5% CO_2 for 2–3 d. Luciferase activities were analyzed with the Dual-Luciferase Reporter System (Beyotime Biotechnology). The Renilla luciferase activities were used as internal controls, and values of firefly luciferase activities were normalized to the corresponding Renilla luciferase activities. All experiments were repeated at least three times.

Analysis of Rac1 activity

hMSCs or hMSCs infected with Sh-P1 or control lentivirus were cultured in normal medium for 5 d. Rac1 activities in equal amounts of protein from the cells were analyzed using a Rac1 G-LISA Rac1 activation assay kit (Cytoskeleton) following the manufacturer's protocol.

Statistical analysis

Statistical analysis was performed using Student's *t* test (two tailed) or one-way ANOVA with Tukey's post-hoc test using GraphPad Prism 7.0. Data are presented as mean ± SEM. A P value <0.05 was considered significant. Data distribution was assumed to be normal, but this was not formally tested.

Online supplemental material

Fig. S1 shows that knockdown of ILK or kindin-2 does not significantly reduce BMPR2 level. Fig. S2 demonstrates that overexpression of BMPR2 promotes OD and inhibits AD. Fig. S3 shows that overexpression of Smurf1 reduces BMPR2 level in HEK293 cells. Fig. S4 shows that inhibition of proteasome or lysosome reverses Smurf-1 overexpression– or PINCH-1 deficiency–induced down-regulation of BMPR2 level. Fig. S5 shows PLA analyses of kindlin-2–Smurf1 and Ki-67–Smurf1 interactions. Table S1 lists primers used for quantitative RT-PCR.

Acknowledgments

This work was supported by the National Natural Science Foundation of China grant 81430068, the Ministry of Science and Technology of China grant 2016YFC1302100, the Natural Science Foundation of Guangdong Province grant 2017B030301018, and the Shenzhen Innovation Committee of Science and Technology grants JCYJ20180302174228311 and ZDSYS20140509142721429.

The authors declare no competing financial interests.

Author contributions: L. Guo, R. Wang, K. Zhang, J. Yuan, J. Wang, X. Wang, and J. Ma conducted the experiments. L. Guo and C. Wu designed the experiments and wrote the paper.

Submitted: 5 February 2019
Revised: 30 June 2019
Accepted: 8 August 2019

References

Aldred, M.A., J. Vijayakrishnan, V. James, F. Soubrier, M.A. Gomez-Sanchez, G. Martensson, N. Galie, A. Manes, P. Corris, G. Simonneau, et al. 2006. BMPR2 gene rearrangements account for a significant proportion of mutations in familial and idiopathic pulmonary arterial hypertension. *Hum. Mutat.* 27:212–213. https://doi.org/10.1002/humu.9398

Andruska, A., and E. Spiekerkoetter. 2018. Consequences of BMPR2 Deficiency in the Pulmonary Vasculature and Beyond: Contributions to Pulmonary Arterial Hypertension. *Int. J. Mol. Sci.* 19. https://doi.org/10.3390/ijms19092499

Aragón, E., N. Goerner, A.I. Zaromytidou, Q. Xi, A. Escobedo, J. Massagué, and M.J. Macias. 2011. A Smad action turnover switch operated by WW domain readers of a phosphoserine code. *Genes Dev.* 25:1275–1288. https://doi.org/10.1101/gad.2060811

Atkinson, C., S. Stewart, P.D. Upton, R. Machado, J.R. Thomson, R.C. Trembath, and N.W. Morrell. 2002. Primary pulmonary hypertension is associated with reduced pulmonary vascular expression of type II bone morphogenetic protein receptor. *Circulation.* 105:1672–1678. https://doi.org/10.1161/01.CIR.0000012754.72951.3D

Beederman, M., J.D. Lamplot, G. Nan, J. Wang, X. Liu, L. Yin, R. Li, W. Shui, H. Zhang, S.H. Kim, et al. 2013. BMP signaling in mesenchymal stem cell differentiation and bone formation. *J. Biomed. Sci. Eng.* 6:32–52. https://doi.org/10.4236/jbise.2013.68A1004

Beppu, H., M. Kawabata, T. Hamamoto, A. Chytil, O. Minowa, T. Noda, and K. Miyazono. 2000. BMP type II receptor is required for gastrulation and early development of mouse embryos. *Dev. Biol.* 221:249–258. https://doi.org/10.1006/dbio.2000.9670

Blank, U., G. Karlsson, and S. Karlsson. 2008. Signaling pathways governing stem-cell fate. *Blood.* 111:492–503. https://doi.org/10.1182/blood-2007-07-075168

Cao, Y., and L. Zhang. 2013. A Smurf1 tale: function and regulation of an ubiquitin ligase in multiple cellular networks. *Cell. Mol. Life Sci.* 70:2305–2317. https://doi.org/10.1007/s00018-012-1170-7

Cao, Y., Q. Lv, and C. Lv. 2015. MicroRNA-153 suppresses the osteogenic differentiation of human mesenchymal stem cells by targeting bone morphogenetic protein receptor type II. *Int. J. Mol. Med.* 36:760–766. https://doi.org/10.3892/ijmm.2015.2275

Chaikuad, A., and A.N. Bullock. 2016. Structural Basis of Intracellular TGF-β Signaling: Receptors and Smads. *Cold Spring Harb. Perspect. Biol.* 8. https://doi.org/10.1101/cshperspect.a022111

Chen, Q., P. Shou, C. Zheng, M. Jiang, G. Cao, Q. Yang, J. Cao, N. Xie, T. Velletri, X. Zhang, et al. 2016. Fate decision of mesenchymal stem cells: adipocytes or osteoblasts? *Cell Death Differ.* 23:1128–1139. https://doi.org/10.1038/cdd.2015.168

Cheng, H., W. Jiang, F.M. Phillips, R.C. Haydon, Y. Peng, L. Zhou, H.H. Luu, N. An, B. Breyer, P. Vanichakarn, et al. 2003. Osteogenic activity of the fourteen types of human bone morphogenetic proteins (BMPs). *J. Bone Joint Surg. Am.* 85:1544–1552. https://doi.org/10.2106/00004623-200308000-00017

Cogan, J.D., M.W. Pauciulo, A.P. Batchman, M.A. Prince, I.M. Robbins, L.K. Hedges, K.C. Stanton, L.A. Wheeler, J.A. Phillips III, J.E. Loyd, and W.C. Nichols. 2006. High frequency of BMPR2 exonic deletions/duplications in familial pulmonary arterial hypertension. *Am. J. Respir. Crit. Care Med.* 174:590–598. https://doi.org/10.1164/rccm.200602-165OC

Cretu, A., P. Castagnino, and R. Assoian. 2010. Studying the effects of matrix stiffness on cellular function using acrylamide-based hydrogels. *J. Vis. Exp.*

Délot, E.C., M.E. Bahamonde, M. Zhao, and K.M. Lyons. 2003. BMP signaling is required for septation of the outflow tract of the mammalian heart. *Development.* 130:209–220. https://doi.org/10.1242/dev.00181

Deng, Z., J.H. Morse, S.L. Slager, N. Cuervo, K.J. Moore, G. Venetos, S. Kalachikov, E. Cayanis, S.G. Fischer, R.J. Barst, et al. 2000. Familial primary pulmonary hypertension (gene PPH1) is caused by mutations in the bone morphogenetic protein receptor-II gene. *Am. J. Hum. Genet.* 67:737–744. https://doi.org/10.1086/303059

Dingal, P.C., and D.E. Discher. 2014. Combining insoluble and soluble factors to steer stem cell fate. *Nat. Mater.* 13:532–537. https://doi.org/10.1038/nmat3997

Du, J., X. Chen, X. Liang, G. Zhang, J. Xu, L. He, Q. Zhan, X.Q. Feng, S. Chien, and C. Yang. 2011. Integrin activation and internalization on soft ECM as a mechanism of induction of stem cell differentiation by ECM elasticity. *Proc. Natl. Acad. Sci. USA.* 108:9466–9471. https://doi.org/10.1073/pnas.1106467108

Dupont, S., L. Morsut, M. Aragona, E. Enzo, S. Giulitti, M. Cordenonsi, F. Zanconato, J. Le Digabel, M. Forcato, S. Bicciato, et al. 2011. Role of YAP/TAZ in mechanotransduction. *Nature.* 474:179–183. https://doi.org/10.1038/nature10137

Fukuda, T., K. Chen, X. Shi, and C. Wu. 2003. PINCH-1 is an obligate partner of integrin-linked kinase (ILK) functioning in cell shape modulation, motility, and survival. *J. Biol. Chem.* 278:51324–51333. https://doi.org/10.1074/jbc.M309122200

Garg, P., M.M. Mazur, A.C. Buck, M.E. Wandtke, J. Liu, and N.A. Ebraheim. 2017. Prospective Review of Mesenchymal Stem Cells Differentiation into Osteoblasts. *Orthop. Surg.* 9:13–19. https://doi.org/10.1111/os.12304

Garimella, R., M.A. Kacena, S.E. Tague, J. Wang, M.C. Horowitz, and H.C. Anderson. 2007. Expression of bone morphogenetic proteins and their receptors in the bone marrow megakaryocytes of GATA-1(low) mice: a possible role in osteosclerosis. *J. Histochem. Cytochem.* 55:745–752. https://doi.org/10.1369/jhc.6A7164.2007

Gomez-Puerto, M.C., P.V. Iyengar, A. Garcia de Vinuesa, P. Ten Dijke, and G. Sanchez-Duffhues. 2019. Bone morphogenetic protein receptor signal transduction in human diseases. *J. Pathol.* 247:9-20.

Guo, L., and C. Wu. 2002. Regulation of fibronectin matrix deposition and cell proliferation by the PINCH-ILK-CH-ILKBP complex. *FASEB J.* 16: 1298–1300. https://doi.org/10.1096/fj.02-0089fje

Guo, L., Y. Zhou, S. Wang, and Y. Wu. 2014. Epigenetic changes of mesenchymal stem cells in three-dimensional (3D) spheroids. *J. Cell. Mol. Med.* 18:2009–2019. https://doi.org/10.1111/jcmm.12336

Guo, L., T. Cai, K. Chen, R. Wang, J. Wang, C. Cui, J. Yuan, K. Zhang, Z. Liu, Y. Deng, et al. 2018. Kindlin-2 regulates mesenchymal stem cell differentiation through control of YAP1/TAZ. *J. Cell Biol.* 217:1431–1451. https://doi.org/10.1083/jcb.201612177

Guo, X., S. Shen, S. Song, S. He, Y. Cui, G. Xing, J. Wang, Y. Yin, L. Fan, F. He, and L. Zhang. 2011. The E3 ligase Smurf1 regulates Wolfram syndrome protein stability at the endoplasmic reticulum. *J. Biol. Chem.* 286: 18037–18047. https://doi.org/10.1074/jbc.M111.225615

Horton, E.R., P. Astudillo, M.J. Humphries, and J.D. Humphries. 2016. Mechanosensitivity of integrin adhesion complexes: role of the consensus adhesome. *Exp. Cell Res.* 343:7–13. https://doi.org/10.1016/j.yexcr.2015.10.025

Huang, C., Z. Rajfur, N. Yousefi, Z. Chen, K. Jacobson, and M.H. Ginsberg. 2009. Talin phosphorylation by Cdk5 regulates Smurf1-mediated talin head ubiquitylation and cell migration. *Nat. Cell Biol.* 11:624–630. https://doi.org/10.1038/ncb1868

Humphrey, J.D., E.R. Dufresne, and M.A. Schwartz. 2014. Mechanotransduction and extracellular matrix homeostasis. *Nat. Rev. Mol. Cell Biol.* 15:802–812. https://doi.org/10.1038/nrm3896

Kavsak, P., R.K. Rasmussen, C.G. Causing, S. Bonni, H. Zhu, G.H. Thomsen, and J.L. Wrana. 2000. Smad7 binds to Smurf2 to form an E3 ubiquitin ligase that targets the TGF beta receptor for degradation. *Mol. Cell.* 6: 1365–1375. https://doi.org/10.1016/S1097-2765(00)00134-9

Kim, M.J., S.Y. Park, H.R. Chang, E.Y. Jung, A. Munkhjargal, J.S. Lim, M.S. Lee, and Y. Kim. 2017. Clinical significance linked to functional defects in bone morphogenetic protein type 2 receptor, BMPR2. *BMB Rep.* 50: 308–317. https://doi.org/10.5483/BMBRep.2017.50.6.059

Korchynskyi, O., and P. ten Dijke. 2002. Identification and functional characterization of distinct critically important bone morphogenetic protein-specific response elements in the Id1 promoter. *J. Biol. Chem.* 277:4883–4891. https://doi.org/10.1074/jbc.M111023200

Kovalevich, J., B. Tracy, and D. Langford. 2011. PINCH: More than just an adaptor protein in cellular response. *J. Cell. Physiol.* 226:940–947. https://doi.org/10.1002/jcp.22437

Lane, K.B., R.D. Machado, M.W. Pauciulo, J.R. Thomson, J.A. Phillips III, J.E. Loyd, W.C. Nichols, R.C. Trembath, and R.C. Trembath. International PPH Consortium. 2000. Heterozygous germline mutations in BMPR2, encoding a TGF-beta receptor, cause familial primary pulmonary hypertension. *Nat. Genet.* 26:81–84. https://doi.org/10.1038/79226

Legate, K.R., E. Montañez, O. Kudlacek, and R. Fässler. 2006. ILK, PINCH and parvin: the tIPP of integrin signalling. *Nat. Rev. Mol. Cell Biol.* 7:20–31. https://doi.org/10.1038/nrm1789

Lehnerdt, G., K.A. Metz, S. Trellakis, K. Jahnke, and A. Neumann. 2007. Signaling by way of type IB and II bone morphogenetic protein receptors regulates bone formation in otospongiosis. *Laryngoscope.* 117: 812–816. https://doi.org/10.1097/MLG.0b013e31803300a2

Li, Y., C. Dai, C. Wu, and Y. Liu. 2007. PINCH-1 promotes tubular epithelial-to-mesenchymal transition by interacting with integrin-linked kinase. *J. Am. Soc. Nephrol.* 18:2534–2543. https://doi.org/10.1681/ASN.2007030315

Li, Z., C. Liu, Z. Xie, P. Song, R.C. Zhao, L. Guo, Z. Liu, and Y. Wu. 2011. Epigenetic dysregulation in mesenchymal stem cell aging and spontaneous differentiation. *PLoS One.* 6:e20526–e20534. https://doi.org/10.1371/journal.pone.0020526

Machado, R.D., N. Rudarakanchana, C. Atkinson, J.A. Flanagan, R. Harrison, N.W. Morrell, and R.C. Trembath. 2003. Functional interaction between BMPR-II and Tctex-1, a light chain of Dynein, is isoform-specific and disrupted by mutations underlying primary pulmonary hypertension. *Hum. Mol. Genet.* 12:3277–3286. https://doi.org/10.1093/hmg/ddg365

MacQueen, L., Y. Sun, and C.A. Simmons. 2013. Mesenchymal stem cell mechanobiology and emerging experimental platforms. *J. R. Soc. Interface.* 10:20130179. https://doi.org/10.1098/rsif.2013.0179

Mammoto, A., and D.E. Ingber. 2009. Cytoskeletal control of growth and cell fate switching. *Curr. Opin. Cell Biol.* 21:864–870. https://doi.org/10.1016/j.ceb.2009.08.001

McBeath, R., D.M. Pirone, C.M. Nelson, K. Bhadriraju, and C.S. Chen. 2004. Cell shape, cytoskeletal tension, and RhoA regulate stem cell lineage commitment. *Dev. Cell.* 6:483–495. https://doi.org/10.1016/S1534-5807(04)00075-9

Miyazono, K., Y. Kamiya, and M. Morikawa. 2010. Bone morphogenetic protein receptors and signal transduction. *J. Biochem.* 147:35–51. https://doi.org/10.1093/jb/mvp148

Murakami, G., T. Watabe, K. Takaoka, K. Miyazono, and T. Imamura. 2003. Cooperative inhibition of bone morphogenetic protein signaling by Smurf1 and inhibitory Smads. *Mol. Biol. Cell.* 14:2809–2817. https://doi.org/10.1091/mbc.e02-07-0441

Murakami, K., R. Mathew, J. Huang, R. Farahani, H. Peng, S.C. Olson, and J.D. Etlinger. 2010. Smurf1 ubiquitin ligase causes downregulation of BMP receptors and is induced in monocrotaline and hypoxia models of pulmonary arterial hypertension. *Exp. Biol. Med. (Maywood).* 235: 805–813. https://doi.org/10.1258/ebm.2010.009383

Narimatsu, M., R. Bose, M. Pye, L. Zhang, B. Miller, P. Ching, R. Sakuma, V. Luga, L. Roncari, L. Attisano, and J.L. Wrana. 2009. Regulation of planar cell polarity by Smurf ubiquitin ligases. *Cell.* 137:295–307. https://doi.org/10.1016/j.cell.2009.02.025

Newman, J.H., R.C. Trembath, J.A. Morse, E. Grunig, J.E. Loyd, S. Adnot, F. Coccolo, C. Ventura, J.A. Phillips III, J.A. Knowles, et al. 2004. Genetic basis of pulmonary arterial hypertension: current understanding and future directions. *J. Am. Coll. Cardiol.* 43(12, Suppl S):33S–39S. https://doi.org/10.1016/j.jacc.2004.02.028

Nie, J., L. Liu, M. Wu, G. Xing, S. He, Y. Yin, C. Tian, F. He, and L. Zhang. 2010. HECT ubiquitin ligase Smurf1 targets the tumor suppressor ING2 for ubiquitination and degradation. *FEBS Lett.* 584:3005–3012. https://doi.org/10.1016/j.febslet.2010.05.033

Noël, D., D. Gazit, C. Bouquet, F. Apparailly, C. Bony, P. Plence, V. Millet, G. Turgeman, M. Perricaudet, J. Sany, and C. Jorgensen. 2004. Short-term BMP-2 expression is sufficient for in vivo osteochondral differentiation of mesenchymal stem cells. *Stem Cells.* 22:74–85. https://doi.org/10.1634/stemcells.22-1-74

Onishi, T., Y. Ishidou, T. Nagamine, K. Yone, T. Imamura, M. Kato, T.K. Sampath, P. ten Dijke, and T. Sakou. 1998. Distinct and overlapping patterns of localization of bone morphogenetic protein (BMP) family members and a BMP type II receptor during fracture healing in rats. *Bone.* 22:605–612. https://doi.org/10.1016/S8756-3282(98)00056-8

Orriols, M., M.C. Gomez-Puerto, and P. Ten Dijke. 2017. BMP type II receptor as a therapeutic target in pulmonary arterial hypertension. *Cell. Mol. Life Sci.* 74:2979–2995. https://doi.org/10.1007/s00018-017-2510-4

Podos, S.D., K.K. Hanson, Y.C. Wang, and E.L. Ferguson. 2001. The DSmurf ubiquitin-protein ligase restricts BMP signaling spatially and temporally during Drosophila embryogenesis. *Dev. Cell.* 1:567–578. https://doi.org/10.1016/S1534-5807(01)00057-0

Qin, J., and C. Wu. 2012. ILK: a pseudokinase in the center stage of cell-matrix adhesion and signaling. *Curr. Opin. Cell Biol.* 24:607–613. https://doi.org/10.1016/j.ceb.2012.06.003

Rooney, N., and C.H. Streuli. 2011. How integrins control mammary epithelial differentiation: a possible role for the ILK-PINCH-Parvin complex. *FEBS Lett.* 585:1663–1672. https://doi.org/10.1016/j.febslet.2011.05.014

Rothman, A.M., N.D. Arnold, J.A. Pickworth, J. Iremonger, L. Ciuclan, R.M. Allen, S. Guth-Gundel, M. Southwood, N.W. Morrell, M. Thomas, et al. 2016. MicroRNA-140-5p and SMURF1 regulate pulmonary arterial hypertension. *J. Clin. Invest.* 126:2495–2508. https://doi.org/10.1172/JCI83361

Schwartz, M.A. 2010. Integrins and extracellular matrix in mechanotransduction. *Cold Spring Harb. Perspect. Biol.* 2:a005066. https://doi.org/10.1101/cshperspect.a005066

Shi, Y., and J. Massagué. 2003. Mechanisms of TGF-beta signaling from cell membrane to the nucleus. *Cell.* 113:685–700. https://doi.org/10.1016/S0092-8674(03)00432-X

Sieber, C., J. Kopf, C. Hiepen, and P. Knaus. 2009. Recent advances in BMP receptor signaling. *Cytokine Growth Factor Rev.* 20:343–355. https://doi.org/10.1016/j.cytogfr.2009.10.007

Tang, Y., R.G. Rowe, E.L. Botvinick, A. Kurup, A.J. Putnam, M. Seiki, V.M. Weaver, E.T. Keller, S. Goldstein, J. Dai, et al. 2013. MT1-MMP-dependent control of skeletal stem cell commitment via a β1-integrin/YAP/TAZ signaling axis. *Dev. Cell.* 25:402–416. https://doi.org/10.1016/j.devcel.2013.04.011

Tu, Y., F. Li, S. Goicoechea, and C. Wu. 1999. The LIM-only protein PINCH directly interacts with integrin-linked kinase and is recruited to integrin-rich sites in spreading cells. *Mol. Cell. Biol.* 19:2425–2434. https://doi.org/10.1128/MCB.19.3.2425

Tu, Y., Y. Huang, Y. Zhang, Y. Hua, and C. Wu. 2001. A new focal adhesion protein that interacts with integrin-linked kinase and regulates cell adhesion and spreading. *J. Cell Biol.* 153:585–598. https://doi.org/10.1083/jcb.153.3.585

Vining, K.H., and D.J. Mooney. 2017. Mechanical forces direct stem cell behaviour in development and regeneration. *Nat. Rev. Mol. Cell Biol.* 18:728–742. https://doi.org/10.1038/nrm.2017.108

Vogel, V., and M.P. Sheetz. 2009. Cell fate regulation by coupling mechanical cycles to biochemical signaling pathways. *Curr. Opin. Cell Biol.* 21:38–46. https://doi.org/10.1016/j.ceb.2009.01.002

Wang, Y.L., and R.J. Pelham Jr. 1998. Preparation of a flexible, porous polyacrylamide substrate for mechanical studies of cultured cells. *Methods Enzymol.* 298:489–496. https://doi.org/10.1016/S0076-6879(98)98041-7

Wang, H.R., Y. Zhang, B. Ozdamar, A.A. Ogunjimi, E. Alexandrova, G.H. Thomsen, and J.L. Wrana. 2003. Regulation of cell polarity and protrusion formation by targeting RhoA for degradation. *Science.* 302:1775–1779. https://doi.org/10.1126/science.1090772

Wang, R.N., J. Green, Z. Wang, Y. Deng, M. Qiao, M. Peabody, Q. Zhang, J. Ye, Z. Yan, S. Denduluri, et al. 2014. Bone Morphogenetic Protein (BMP) signaling in development and human diseases. *Genes Dis.* 1:87–105. https://doi.org/10.1016/j.gendis.2014.07.005

Wang, S., L. Guo, J. Ge, L. Yu, T. Cai, R. Tian, Y. Jiang, R.Ch. Zhao, and Y. Wu. 2015. Excess Integrins Cause Lung Entrapment of Mesenchymal Stem Cells. *Stem Cells.* 33:3315–3326. https://doi.org/10.1002/stem.2087

Wei, X., X. Wang, J. Zhan, Y. Chen, W. Fang, L. Zhang, and H. Zhang. 2017. Smurf1 inhibits integrin activation by controlling Kindlin-2 ubiquitination and degradation. *J. Cell Biol.* 216:1455–1471. https://doi.org/10.1083/jcb.201609073

Wickström, S.A., A. Lange, E. Montanez, and R. Fässler. 2010. The ILK/PINCH/parvin complex: the kinase is dead, long live the pseudokinase! *EMBO J.* 29:281–291. https://doi.org/10.1038/emboj.2009.376

Wozniak, M.A., and C.S. Chen. 2009. Mechanotransduction in development: a growing role for contractility. *Nat. Rev. Mol. Cell Biol.* 10:34–43. https://doi.org/10.1038/nrm2592

Wu, C. 2004. The PINCH-ILK-parvin complexes: assembly, functions and regulation. *Biochim. Biophys. Acta.* 1692:55–62. https://doi.org/10.1016/j.bbamcr.2004.01.006

Wu, C. 2005. PINCH, N(i)ck and the ILK: network wiring at cell-matrix adhesions. *Trends Cell Biol.* 15:460–466. https://doi.org/10.1016/j.tcb.2005.07.002

Wu, C., and S. Dedhar. 2001. Integrin-linked kinase (ILK) and its interactors: a new paradigm for the coupling of extracellular matrix to actin cytoskeleton and signaling complexes. *J. Cell Biol.* 155:505–510. https://doi.org/10.1083/jcb.200108077

Wu, C., H. Jiao, Y. Lai, W. Zheng, K. Chen, H. Qu, W. Deng, P. Song, K. Zhu, H. Cao, et al. 2015. Kindlin-2 controls TGF-β signalling and Sox9 expression to regulate chondrogenesis. *Nat. Commun.* 6:7531. https://doi.org/10.1038/ncomms8531

Wu, N., Y. Zhao, Y. Yin, Y. Zhang, and J. Luo. 2010. Identification and analysis of type II TGF-β receptors in BMP-9-induced osteogenic differentiation of C3H10T1/2 mesenchymal stem cells. *Acta Biochim. Biophys. Sin. (Shanghai).* 42:699–708. https://doi.org/10.1093/abbs/gmq075

Wu, Y., L. Chen, P.G. Scott, and E.E. Tredget. 2007. Mesenchymal stem cells enhance wound healing through differentiation and angiogenesis. *Stem Cells.* 25:2648–2659. https://doi.org/10.1634/stemcells.2007-0226

Xie, P., Y. Tang, S. Shen, Y. Wang, G. Xing, Y. Yin, F. He, and L. Zhang. 2011. Smurf1 ubiquitin ligase targets Kruppel-like factor KLF2 for ubiquitination and degradation in human lung cancer H1299 cells. *Biochem. Biophys. Res. Commun.* 407:254–259. https://doi.org/10.1016/j.bbrc.2011.03.016

Yadav, P.S., P. Prashar, and A. Bandyopadhyay. 2012. BRITER: a BMP responsive osteoblast reporter cell line. *PLoS One.* 7:e37134. https://doi.org/10.1371/journal.pone.0037134

Yamaguchi, K., O. Ohara, A. Ando, and T. Nagase. 2008. Smurf1 directly targets hPEM-2, a GEF for Cdc42, via a novel combination of protein interaction modules in the ubiquitin-proteasome pathway. *Biol. Chem.* 389:405–413. https://doi.org/10.1515/BC.2008.036

Yamashita, M., S.X. Ying, G.M. Zhang, C. Li, S.Y. Cheng, C.X. Deng, and Y.E. Zhang. 2005. Ubiquitin ligase Smurf1 controls osteoblast activity and bone homeostasis by targeting MEKK2 for degradation. *Cell.* 121:101–113. https://doi.org/10.1016/j.cell.2005.01.035

Yang, C., L. Yang, M. Wan, and X. Cao. 2010. Generation of a mouse model with expression of bone morphogenetic protein type II receptor lacking the cytoplasmic domain in osteoblasts. *Ann. N. Y. Acad. Sci.* 1192:286–291. https://doi.org/10.1111/j.1749-6632.2009.05248.x

Yang, Y., L. Guo, S.M. Blattner, P. Mundel, M. Kretzler, and C. Wu. 2005. Formation and phosphorylation of the PINCH-1-integrin linked kinase-alpha-parvin complex are important for regulation of renal glomerular podocyte adhesion, architecture, and survival. *J. Am. Soc. Nephrol.* 16:1966–1976. https://doi.org/10.1681/ASN.2004121112

Yim, E.K., and M.P. Sheetz. 2012. Force-dependent cell signaling in stem cell differentiation. *Stem Cell Res. Ther.* 3:41. https://doi.org/10.1186/scrt132

Ying, S.X., Z.J. Hussain, and Y.E. Zhang. 2003. Smurf1 facilitates myogenic differentiation and antagonizes the bone morphogenetic protein-2-induced osteoblast conversion by targeting Smad5 for degradation. *J. Biol. Chem.* 278:39029–39036. https://doi.org/10.1074/jbc.M301193200

Yuan, C., J. Qi, X. Zhao, and C. Gao. 2012. Smurf1 protein negatively regulates interferon-γ signaling through promoting STAT1 protein ubiquitination and degradation. *J. Biol. Chem.* 287:17006–17015. https://doi.org/10.1074/jbc.M112.341198

Zeng, Y., X. Qu, H. Li, S. Huang, S. Wang, Q. Xu, R. Lin, Q. Han, J. Li, and R.C. Zhao. 2012. MicroRNA-100 regulates osteogenic differentiation of human adipose-derived mesenchymal stem cells by targeting BMPR2. *FEBS Lett.* 586:2375–2381. https://doi.org/10.1016/j.febslet.2012.05.049

Zhang, J., and L. Li. 2005. BMP signaling and stem cell regulation. *Dev. Biol.* 284:1–11. https://doi.org/10.1016/j.ydbio.2005.05.009

Zhang, Y., L. Guo, K. Chen, and C. Wu. 2002. A critical role of the PINCH-integrin-linked kinase interaction in the regulation of cell shape change and migration. *J. Biol. Chem.* 277:318–326. https://doi.org/10.1074/jbc.M108257200

Zhao, M., M. Qiao, B.O. Oyajobi, G.R. Mundy, and D. Chen. 2003. E3 ubiquitin ligase Smurf1 mediates core-binding factor alpha1/Runx2 degradation and plays a specific role in osteoblast differentiation. *J. Biol. Chem.* 278:27939–27944. https://doi.org/10.1074/jbc.M304132200

Zhu, H., P. Kavsak, S. Abdollah, J.L. Wrana, and G.H. Thomsen. 1999. A SMAD ubiquitin ligase targets the BMP pathway and affects embryonic pattern formation. *Nature.* 400:687–693. https://doi.org/10.1038/23293